frontiers | Frontiers in Environmental Science

TYPE Original Research
PUBLISHED 17 October 2022
DOI 10.3389/fenvs.2022.995190

OPEN ACCESS

EDITED BY
Meilian Chen,
Guangdong Technion—Israel Institute of Technology, China

REVIEWED BY
Liyang Yang,
Fuzhou University, China
Wei He,
China University of Geosciences, China
Morgane Derrien,
Universidad de O'Higgins, Rancagua, Chile

*CORRESPONDENCE
Chao Wang,
chaowang@gdou.edu.cn
Guangzhe Jin,
jinguangzhe@live.cn

SPECIALTY SECTION
This article was submitted to Biogeochemical Dynamics, a section of the journal Frontiers in Environmental Science

RECEIVED 15 July 2022
ACCEPTED 03 October 2022
PUBLISHED 17 October 2022

CITATION
Wang C, Hu X, Liu Y and Jin G (2022), Sources, spectral characteristics, and fluxes of dissolved organic matter in coastal groundwater and river water in western Guangdong, China.
Front. Environ. Sci. 10:995190.
doi: 10.3389/fenvs.2022.995190

Sources, spectral characteristics, and fluxes of dissolved organic matter in coastal groundwater and river water in western Guangdong, China

Chao Wang[1,2,3,4]*, Xuanyu Hu[1], Yilin Liu[1] and Guangzhe Jin[1,3,4]*

[1]Laboratory for Coastal Ocean Variation and Disaster Prediction, College of Ocean and Meteorology, Guangdong Ocean University, Zhanjiang, China, [2]Guangxi Key Laboratory of Beibu Gulf Marine Resources, Environment and Sustainable Development, Fourth Institute of Oceanography, Ministry of Natural Resources, Beihai, China, [3]Key Laboratory of Climate, Resources and Environment in Continental Shelf Sea and Deep Sea of Department of Education of Guangdong Province, Guangdong Ocean University, Zhanjiang, China, [4]Key Laboratory of Space Ocean Remote Sensing and Application, Ministry of Natural Resources, Beijing, China

Groundwater discharge and river runoff are two important ways for allochthonous dissolved organic matter (DOM) to enter the ocean, but they vary spatially. Currently, the source, composition, and efflux of groundwater and riverine dissolved organic matter to the tropical northern South China Sea remain poorly understood, preventing an accurate estimate of coastal carbon budgets. In July 2021, nine groundwater and six river water samples were collected along the coast of western Guangdong and were characterized using dissolved organic carbon (DOC) analysis, UV-visible, and fluorescence spectroscopy techniques. Atypical absorption spectra were strongly observed in groundwaters, which were mainly attributed to the high-level nitrates. An exponential-Gaussian equation showed that the average contribution of nitrate to total groundwater absorbances was up to 36% at ~ 300 nm. Groundwater showed lower levels of DOC, colored dissolved organic matter (CDOM), and fluorescent dissolved organic matter (FDOM) as compared to river water, whereas the humic-like components dominated both groundwater and river water FDOM pools. Higher values of spectral slope $S_{350-400}$, fluorescence index, biological index, and the ratio of two humic-like fluorescence jointly reveal that groundwater DOM mainly originated from microbial activities, whereas the river water DOM had considerable contribution from terrestrial soil. High precipitation, natural or agricultural land types, and a lack of seawater intrusion are expected to cause low levels of groundwater DOM in western Guangdong. Among 52 rivers from across the globe, high watershed productivity and precipitation may lead to high–moderate DOM levels in river water in western Guangdong. The DOM fluxes *via* fresh groundwater discharge in western Guangdong are comparable in magnitude to those by river runoff, accounting for 16%–18% of the Pearl River DOM fluxes. Based on the slopes of linear correlations between CDOM and DOC obtained in groundwater samples and 52 rivers, as well as the data on water fluxes and DOC levels, the

global CDOM fluxes *via* groundwater discharge and river runoff are estimated to be 3.5–12.2 × 10^{12} m^2 yr^{-1} and 4.3 ± 0.3 × 10^{14} m^2 yr^{-1}, respectively, highlighting the importance of considering groundwater discharge and river runoff in coastal carbon budgets.

KEYWORDS

western Guangdong, groundwater, river water, dissolved organic carbon, colored dissolved organic matter, fluorescent dissolved organic matter, flux

1 Introduction

Marine dissolved organic matter (DOM) is one of the largest organic carbon pools on Earth (~662 Pg C), which is equivalent to atmospheric CO_2 (Hansell et al., 2009; Collins et al., 2013). Besides *in situ* biological productions, external sources, such as river runoff and subterranean groundwater discharge (SGD), play an important role in shaping the DOM budget in coastal regions (Carlson and Hansell, 2015). These allochthonous sources show large diversities in terms of the level, composition, export flux, and biogeochemical activity of DOM, resulting in distinct fates and profound implications for coastal ecosystems (Raymond and Spencer, 2015; Shen et al., 2015; Wang et al., 2018). Moreover, climate change (e.g., global warming, extreme climatic events) and human activities (e.g., damming, urbanization) have dramatically changed the composition, reactivity, and export flux of riverine (Liu et al., 2020; Qu et al., 2020, 2022) and groundwater DOM (Lipczynska-Kochany, 2018; McDonough et al., 2020a) delivered to sea. It is, therefore, crucial to determine the quantity, quality, and export flux of DOM at the dynamic land–sea interface, to provide a basis for a better understanding of the coastal biogeochemistry on a changing Earth.

Groundwater stores most of the liquid freshwater on Earth (Ferguson et al., 2021). It is a major source of water and DOM for coastal seas, especially those without input from large rivers (Dai et al., 2021). Early studies on groundwater focused on the level and source of DOM in groundwater (Leenheer et al., 1974; Kalbitz et al., 2000), but increasing information is now available on the bioavailability (Shen et al., 2015), transformation (McDonough et al., 2022), and export flux of groundwater DOM (Yang et al., 2015; Dai et al., 2021). Its response to changing environments is also better understood in recent years (McDonough et al., 2020a, b). Groundwater DOM, consisting of tens of thousands of formulae (McDonough et al., 2020c, 2022), generally originates from the direct infiltration of surface DOM, plant litter, and soil (Baker et al., 2000; Kalbitz et al., 2000; Shen et al., 2015) and its environmental or microbial transformation (Donn and Barron, 2013) or water–rock interactions (Walter et al., 2017). Additionally, human activities (e.g., agriculture, urbanization) provide additional organic molecules to the DOM pools preserved in the aquifers, resulting in remarkable alterations in the composition, transformation, and fate of groundwater DOM (Wang et al., 2013). The increasing reliance on groundwater due to global population growth and climate change may further intensify changes in the DOM cycle of the groundwater system (Wada, 2016). Globally, the groundwater DOC concentration ranges from <40 μmol L^{-1} to >1,000 μmol L^{-1} and varies spatially (Yang et al., 2015; Chen et al., 2018), which is attributed to multiple factors, including aquifer type, temperature, precipitation, water chemical conditions, and land use (McDonough et al., 2020a). The large variability in groundwater recharge, DOM level, and diverse influencing factors suggest that more studies are needed to precisely quantify the export flux of DOM to the ocean *via* SGD and better evaluate its impact on the global carbon cycle (Maher et al., 2013; Kwon et al., 2014).

Absorption and fluorescence spectroscopies are effective techniques for tracing DOM transport from the watershed to the open ocean (Baker, 2001; Guo et al., 2014; Li et al., 2019; Wang et al., 2021; Qu et al., 2022). They are thus widely used to characterize the sources, levels, composition, and flux of colored and fluorescent DOM (CDOM and FDOM) in groundwater (Chen et al., 2010; Tedetti et al., 2011; Nelson et al., 2015; Kim and Kim, 2017). Webb et al. (2019) determined high variability in SGD-derived DOC and CDOM fluxes in 12 coastal systems in eastern Australia and Cook Island, including tidal freshwater wetlands, estuaries, mangroves, coral reefs, coastal lakes, a saltmarsh, and a residential canal estate. Kim and Kim (2017) found that SGD dilutes DOC and protein-like FDOM in the coastal water off Jeju Island, while enhancing the inventory of humic-like FDOM storage in seawater by 2–3 times. Due to dark conditions, SGD-derived DOM tends to have a high potential for photochemical degradation in the coastal sea. Carlson and Wiegner (2016) speculated that the photochemical enhancement of the bioavailability of DOC in some SGD plumes along the coast of Hawai'i Island may facilitate the growth of the bacterial community in the plumes. Qi et al. (2018) confirmed that the efficiencies of CDOM photobleaching and DOC photodegradation in coastal groundwater were significantly higher than in inland groundwater along the Gulf of St. Lawrence. As the photolabile DOM entered the sea *via* SGD, they could be quickly transported to the surface (e.g., due to buoyancy and physical mixing) and participate in the coastal carbon cycle through photochemical and microbial degradation

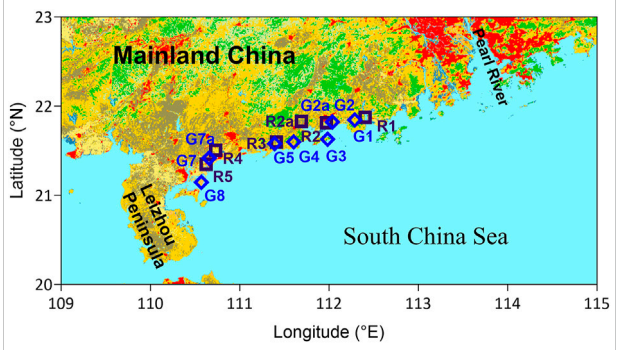

FIGURE 1
Map of the sampling stations. Squares represent river water samples and diamonds represent groundwater samples. Background color represents land use type in 2016: red color represents urban residence; Green color represents natural forest vegetation; Yellow color gray represents agricultural land (data source: https://earthdata.nasa.gov/). The identification of river water samples is as follows: R1, Nafu River; R2, Moyang River; R2a, Huangshi River; R3, Rudong River; R4 and R5, Jian River.

(Fichot and Benner, 2014). Moreover, due to strong soil mineral interaction and microbial activities, there is usually a high concentration of iron (trivalent) and nitrate in groundwater (Arslan et al., 2017). Iron and nitrate may absorb UV and visible light, resulting in a large error in quantifying groundwater CDOM concentration and its flux into the sea. However, this possibility has received little attention in previous studies on groundwater CDOM (Qi et al., 2018).

In this study, we aim to 1) determine the levels and sources of DOC, CDOM, and FDOM in the groundwater and river water from the western coast of Guangdong, China, where the discharge of groundwater is fast but river runoff is relatively slow, 2) identify and distinguish the interferences of nitrate and iron on CDOM absorption spectra in groundwater using additional experiments and an exponential-Gaussian equation, 3) estimate the fluxes of DOC, CDOM, and FDOM *via* SGD and river runoff, and 4) highlight the importance of these fluxes by comparing with other data from the world.

2 Materials and methods

2.1 Study area

The western coast of Guangdong, China is located at the west of the Pearl River estuary, with a coast length of ~2,314 km (Tan et al., 2018). The land in the study area is mainly used for agriculture, human habitation, forestland, and aquaculture (Figure 1). Due to the influence of monsoons and typhoons, the annual precipitation on the western coast of Guangdong is up to ~1800 mm (Chen et al., 2021). The Jianjiang and Moyang Rivers, with an average discharge of 8.98×10^9 and 8.59×10^9 m^3 yr^{-1} to the northwestern shelf of SCS, respectively, are two major rivers on the west coast of Guangdong. Other small rivers, such as the Rudong, Nafu, and Huangshi Rivers, together contribute <5% of total river runoff in the study area. Using a three end-member mixing model and a Ra box model, Tan et al. (2018) reported that SGD flux on the western coast of Guangdong is up to 2.0×10^{11} m^3 yr^{-1}, which is ~11 times the total flux of rivers on the western coast of Guangdong. It should be noted that the SGD flux is composed mainly of recirculated seawater (>90%, Tan et al., 2018; Dai et al., 2021).

2.2 Sampling

Nine groundwater samples and six river water samples were collected along the western coast of Guangdong on July 16–17, 2021 (Figure 1). The groundwater samples were pumped from the wells, and the river water samples were collected using a Niskin bottle at a depth of ~0.5 m below the surface. After collection, the samples were filtered through MF-Millipore™ filters (pore size: 0.45 μm) and stored frozen until analysis for nitrate, nitrite, and total dissolved iron. Samples for DOC, CDOM, and FDOM analyses were filtered immediately through pre-combusted (500°C, 5 h) GF/F filters (Whatman, nominal pore size = 0.7 μm) into pre-combusted glass vials. DOC samples were acidified with H_3PO_4 (85%, Merck) to pH < 2 and kept frozen until analysis. CDOM and FDOM samples were stored in the dark at 4°C. All analyses were finished within 2 days after sampling.

2.3 Salinity, nitrate, nitrite, and iron analyses

The salinity of groundwater and river water samples was measured using a Thermo Scientific™ Elite CTS tester (salinity resolution of 0.10 ppt). Nitrate and nitrite concentrations of groundwater and river water samples were determined using a San^{++} continuous flow analyzer (Skalar, Netherlands). The quantification limit was 0.1 μmol L^{-1} for the sum of nitrate and nitrite. The concentrations of total dissolved iron in groundwater and river water samples were measured using a 7500cx ICP-MS (Agilent, United States) with a detection limit of ~0.015 μmol L^{-1} according to the Chinese standard: water quality-determination of 65 elements–inductively coupled plasma–mass spectrometry (HJ 700–2014).

2.4 Dissolved organic carbon analysis

DOC concentrations of 15 groundwater and river water samples were measured in triplicate using an Elementar Vario

TOC cube (Germany) in high-temperature catalytic oxidation mode with the coefficients of variance <2% (Wang et al., 2021). A five-point standard curve was generated using potassium hydrogen phthalate standards. The running blank was determined as the average of the peak area of the Milli-Q water acidified with H_3PO_4. DOC concentrations were obtained by subtracting the running blank from the average peak area of the samples (injected 3–5 times) and dividing by the slope of the standard curve. The analytical precision of the DOC analysis was <3% based on the consensus reference material (CRM) provided by Hansell Lab from the University of Miami (https://hansell-lab.rsmas.miami.edu/consensus-reference-material/index.html).

2.5 Colored dissolved organic matter measurements and data processing

The absorbance spectra (240–800 nm; A_λ) for groundwater and river water samples were measured using a Shimadzu UV–Visible 1780 dual beam spectrophotometer and 10-cm quartz cuvettes at room temperature. The fresh Milli-Q water was measured to provide a blank to correct for any baseline drift. Absorbance was corrected by subtracting the absorbance of Milli-Q water, which was then converted to a Napierian absorption coefficient, a_λ (m^{-1}) using the following equation:

$$a_\lambda = 2.303A_\lambda/0.1 \quad (1)$$

The spectral slope over 350–400 nm ($S_{350-400}$, nm^{-1}) was calculated based on the nonlinear fit of an exponential function of the absorption spectrum (Eq. 2) over the wavelength range (Helms et al., 2008).

$$a_\lambda = a_{\lambda_0} e^{-S(\lambda-\lambda_0)} + K \quad (2)$$

where λ_0 is the reference wavelength (nm), and K is a background constant (m^{-1}) accounting for scattering in the cuvette and drift of the instrument. Owing to the potential effect of inorganic matter on the CDOM absorption coefficient, the specific ultraviolet absorbance at 350 nm ($SUVA_{350}$) was calculated by dividing the absorbance measured at 350 nm in inverse meters (m^{-1}) by the concentration of DOC; the $SUVA_{350}$ was reported in units of $m^2\ g^{-1}$ C (Weishaar et al., 2003; Hansen et al., 2016).

2.6 Fluorescent dissolved organic matter measurements and data processing

Excitation–emission matrices (EEMs) for all samples were made on an F-7100 spectrofluorometer (Hitachi, Japan) with a 1-cm quartz cuvette at room temperature. The excitation (Ex) wavelengths spanned from 240 to 450 nm with 5-nm intervals, and the emission (Em) wavelengths ranged from 280 to 600 nm with 2-nm intervals. The slit widths for excitation and emission were set to 5 nm. After the sample was analyzed, the Milli-Q water blank was subtracted to remove Raman and Rayleigh scatterings, and the fluorescence intensity was normalized to Raman Unit (RU) according to the method of Lawaetz and Stedmon (2009). The normalized EEMs were then calibrated for inner filter effects using an absorbance-based approach (Kothawala et al., 2013). Fifteen normalized and calibrated EEMs were decomposed into several components using parallel factor analysis (PARAFAC) on the MATLAB 2016b platform using the DOMFluor toolbox (Stedmon and Bro, 2008; Wang et al., 2017). Split-half analyses were performed to validate the number of components obtained based on a randomized split of the dataset (Stedmon and Bro, 2008). To enhance the robustness and confidence of the PARAFAC model, a comparison was performed between our results and the published fluorescent components from the online OpenFluor database (https://openfluor.lablicate.com/, last access: 9 September 2022; Murphy et al., 2014).

Three fluorescence parameters based on the EEMs were used to indicate the sources, composition, and reactivity of DOM. The fluorescence index (FI) was calculated as the ratio of the emission intensity at 470 nm to that at 520 nm, obtained with an excitation at 370 nm (Cory and McKnight, 2005). The humification index (HIX) was calculated as the integrated emission spectra at 435–480 nm divided by that at 300–345 nm, upon excitation at 254 nm (Zsolnay et al., 1999). The biological index (BIX) was calculated as the ratio of fluorescence intensity emitted at 380 nm to the intensity emitted at 430 nm, upon 310 nm (Huguet et al., 2009). Moreover, the ratio of humic-like fluorescence to protein-like fluorescence (H/P) was calculated as the sum of the intensities of all humic-like components divided by the total intensity of protein-like components (Hansen et al., 2016). The ratio of fluorescence intensity of traditionally "marine" and "terrestrial" humic-like components was also reported in this study (Yamashita et al., 2010; Wang et al., 2017).

2.7 Nitrate addition experiments

To assess the impact of nitrate on the absorption spectra of groundwater and river water samples, we conducted a series of nitrate addition experiments. Four representative samples were selected based on the initial nitrate concentrations, including two groundwater (G2, G5) and two river water (R1, R2) samples with minimal and maximum nitrate concentrations, respectively. Different amounts of sodium nitrate (ACS reagent, Sigma-Aldrich) were added to these samples to achieve the additional nitrate concentrations of 0, 200, 500, 1,000, and 2,000 μmol L^{-1}, respectively. The absorption curves of these 'new' samples were then obtained using the conventional method described in Section 2.5.

TABLE 1 Salinity, nitrate, nitrite, and total dissolved iron in nine groundwater and six river water samples.

Station	Description	Salinity	Nitrate (μmol L^{-1})	Nitrite (μmol L^{-1})	Total dissolved iron (μmol L^{-1})
G1	Groundwater	0	69.94	0.05	0.04
G2	Groundwater	0	1,287.47	0.04	0.04
G2a	Groundwater	0	1,014.70	0.02	0.16
G3	Groundwater	0	713.06	0.90	0.10
G4	Groundwater	0	684.86	0.17	0.05
G5	Groundwater	0	274.71	0.06	0.28
G7	Groundwater	0	246.42	0.04	0.07
G7a	Groundwater	0	611.95	0.67	0.05
G8	Groundwater	0	1,162.67	0.82	0.04
R1	River water	0	30.67	25.90	0.09
R2	River water	0	90.52	12.47	0.37
R2a	River water	0	52.32	4.74	0.42
R3	River water	0	49.02	7.16	0.79
R4	River water	0	102.30	22.48	0.26
R5	River water	0	36.98	7.88	0.23

2.8 Calculations of dissolved organic matter fluxes *via* groundwater discharge and river runoff

The fluxes of DOC, CDOM, and FDOM exported to the northern South China Sea by fresh groundwater discharge and river runoff were estimated as follows (Tan et al., 2018; Li et al., 2019; Dai et al., 2021):

$$F = Q \times C \quad (3)$$

where F denotes the flux of DOC or CDOM or FDOM; Q represents the fresh groundwater discharge rate or river runoff, and C indicates the average concentrations of DOC or CDOM or the average intensity of FDOM components in groundwater or river water samples. The fresh groundwater discharge rate in the research region was estimated to be 4.74×10^{10} m^3 yr^{-1} according to the method of Zhang and Li (2005) and Tan et al. (2018). Data on the river runoff in western Guangdong (Jian River, Moyang River, and Rudong River) were made available by the Water Resources Department of Guangdong Province, China (http://slt.gd.gov.cn/yszx/).

2.9 Statistical analyses

The significance of DOM comparisons between groundwater and river water samples was tested using a t-test (two-tailed, $\alpha = 0.05$) in IBM SPSS Statistics 23. Pearson correlation analyses among the DOM and environmental variables were performed using OriginPro 2022b and the significant level (p-value) was determined by a two-tailed test.

3 Results

3.1 Distributions of salinity, nitrate, nitrite, and total dissolved iron

Table 1 shows salinity, nitrate, nitrite, and total dissolved iron content in groundwater and river water samples. N salinity was observed in the groundwater and river water samples. The nitrate concentrations in nine groundwater samples ranged from 69.9 to 1,288 μmol L^{-1} in groundwater, with average nitrate of 674 ± 424 μmol L^{-1}. Nitrate concentrations in six river samples varied from 29.3 to 102.3 μmol L^{-1} where the mean value (60.3 ± 29.3 μmol L^{-1}) was less than one-tenth of that in groundwater samples. On the contrary, nitrite concentrations were much lower in groundwater samples (0.04–0.90 μmol L^{-1}) as compared to those in river samples (4.7–25.9 μmol L^{-1}). The concentrations of total dissolved iron ranged from 0.05 to 0.79 μmol L^{-1} in all samples, with an average of 0.09 ± 0.08 μmol L^{-1} and 0.36 ± 0.24 μmol L^{-1} in groundwater and river waters, respectively (Table 1).

3.2 Distributions of dissolved organic carbon and chromophoric dissolved organic matter

The groundwater DOC concentrations ranged from 29 to 190 μmol L^{-1} with an average of 93.6 ± 62.3 μmol L^{-1}. DOC concentration in river waters varied between 221 and 442 μmol L^{-1} with a higher average value (311 ± 77.5 μmol L^{-1}) than that in groundwaters (t-test, $p < 0.001$, Figure 2A). The absorption coefficient

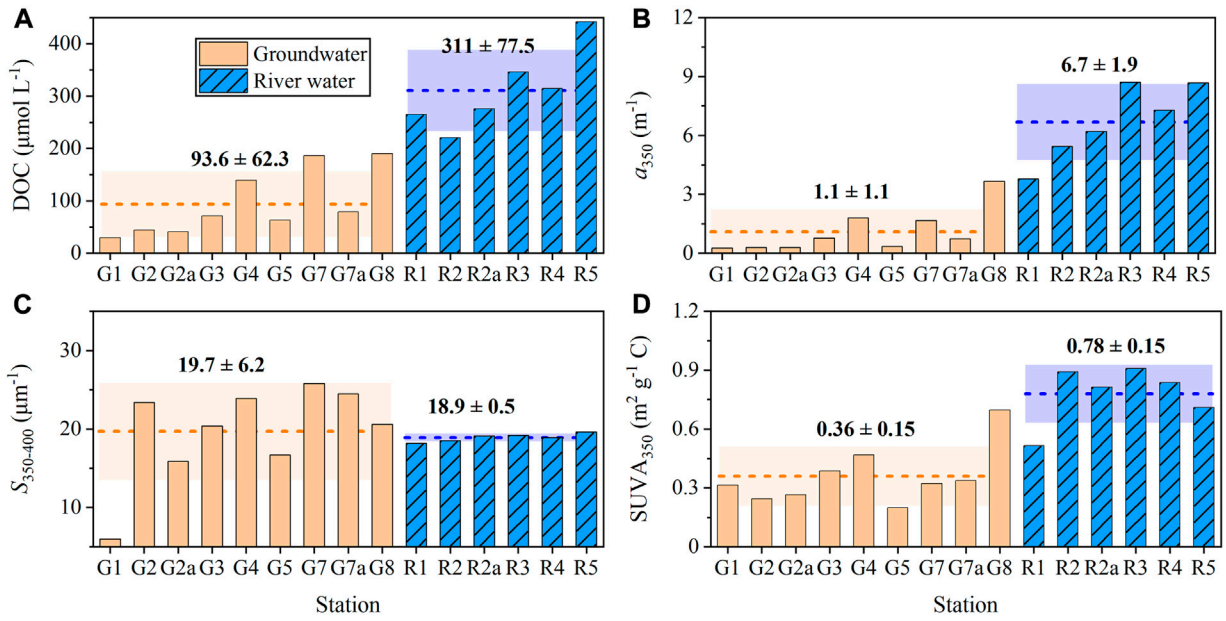

FIGURE 2
Distributions of **(A)** DOC, **(B)** a_{350}, **(C)** $S_{350-400}$ and **(D)** $SUVA_{350}$ in groundwater and river water samples. The dotted lines and shadows denote the average values and standard deviations, respectively.

at 350 nm (a_{350}) of groundwater and river water samples ranged from 0.25 to 3.66 m^{-1} and 3.78–8.71 m^{-1}, respectively, and was linearly correlated to DOC concentration (R^2 = 0.92, p < 0.001, n = 15, Supplementary Figure S1A). As compared to the river water samples, groundwater showed lower CDOM concentrations (t-test, p < 0.001, Figure 2B). The groundwater spectral slope, $S_{350-400}$, ranged from 6.0 to 25.8 μm^{-1} with an average value of 19.7 ± 6.2 μm^{-1}. The average of $S_{350-400}$ in river waters (18.9 ± 0.5 μm^{-1}) was comparable to that in groundwaters but varied on a smaller scale from 18.2 to 19.6 μm^{-1} at different stations (Figure 2C). The variation range of $SUVA_{350}$ values was 0.20–0.70 $m^2\ g^{-1}$ C for groundwater samples and 0.52–0.91 $m^2\ g^{-1}$ C for river water samples (Figure 2D). Groundwaters showed a lower average $SUVA_{350}$ value (0.36 ± 0.15 $m^2\ g^{-1}$ C) than river waters (0.78 ± 0.15 $m^2\ g^{-1}$ C, t-test, p < 0.001).

3.3 PARAFAC results

PARAFAC modeling resulted in a five-component model that explained >99% of the variability among the EEMs, including three humic-like components (C1–C3) and two protein-like components (C4 and C5) (Figure 3). The comparisons to the online OpenFluor spectral database (Murphy et al., 2014) show that five FDOM components in this study are similar to PARAFAC-derived components identified in previously published studies. In these cases, the Tucker congruence coefficient (TCC) exceeded 0.95 on the excitation and emission spectra simultaneously. C1 displayed two excitation maxima at ≤ 240 and 300 nm and one emission maximum at 400 nm. Similar fluorescence signatures were previously categorized to represent a mixture of humic-like peak A and marine humic-like peak M (Coble, 1996). C1 presented 56 pairs of matches in the online comparison, including components found in various aquatic environments, such as seawater (Kowalczuk et al., 2013; Catalá et al., 2015), river and estuarine waters (Guo et al., 2011), and groundwater (Wang et al., 2013; Yang et al., 2015), which were tightly related to *in situ* microbial activities (Wang et al., 2021). C2 displayed two excitation maxima at 250 and 340 nm and one emission maxima at 448 nm. Similar fluorescence signatures have previously been categorized to originate from a mixture of terrestrial humic-like fluorescence peaks A and C (Coble, 1996). C3 had an excitation/emission maximum at 270/460 nm, which was similar to common humic-like peak A. Matches for C2 and C3 were found in seven and four published models, respectively. However, these components are ubiquitously found in aquatic DOM from watershed to deep ocean continuum (Wang et al., 2013, 2021; Qu et al., 2022). C4 had excitation/emission maxima at ≤ 240 and 275 nm/340 nm, which is consistent with tryptophan-like peak T (Coble, 1996). C4 was demonstrated to be a good proxy of freshly phytoplankton-derived and anthropogenic DOM (Guo et al., 2014). Fifty online spectra matching C4 were obtained, including spectra from natural aquatic environments, such as

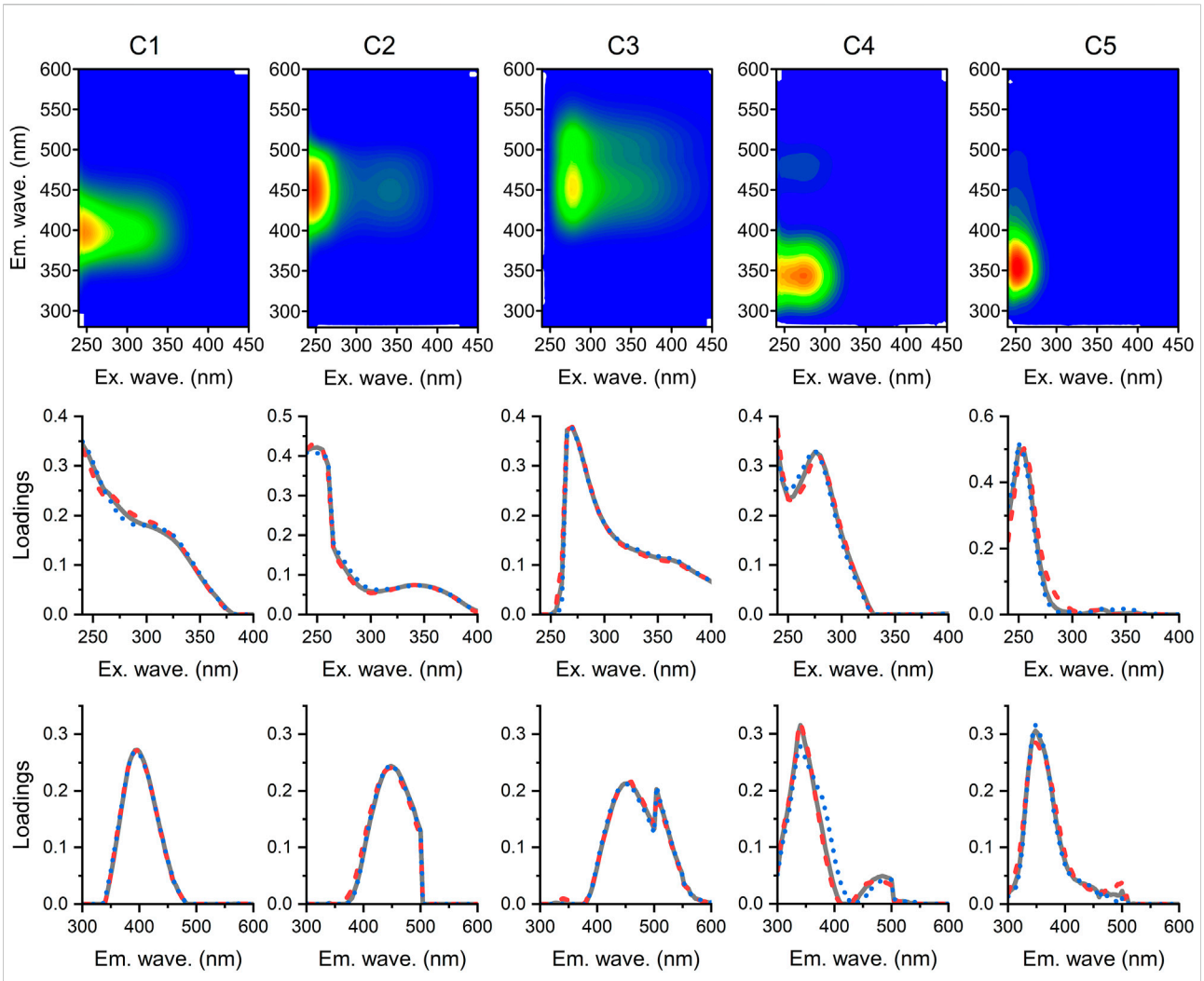

FIGURE 3
Fluorescence signatures of five PARAFAC components (C1–C5) identified in the groundwater and river water EEMs dataset (top row). Line plots show split-half validations in which each component's excitation (middle row) and emission loadings (bottom row) are produced from two independent halves of the dataset (dashed and dotted lines) and the complete dataset (solid lines).

river water, groundwater, and seawater (Guo et al., 2014; Yang et al., 2015; Wang et al., 2017), and engineered systems (Moona et al., 2021). C5 showed excitation/emission maxima at 250 nm/348 nm and covered the fluorescence region of tryptophan-like fluorophores (Coble, 1996). It matched only two components in the online database, including C5 in Wünsch et al. (2015) and C4 in Wang et al. (2020).

3.4 Distributions of fluorescent dissolved organic matter

Three humic-like components (C1–C3) showed good linear correlations in pairs ($R^2 > 0.96$, $p < 0.001$, $n = 15$, Supplementary Figures S2A–C). The total intensities of the three humic-like components in groundwaters spanned two orders of magnitude, from 0.013 to 3.21 RU, with an average intensity of 0.78 ± 1.01 RU. By comparison, the total intensities of the three humic-like components in river waters were much higher (1.81 ± 0.70 RU) and varied in a smaller range (0.79–2.81 RU, Figures 4A–C). The intensity of protein-like C4 varied from 0.028 to 0.42 RU in groundwaters and from 0.24 to 0.42 RU in river waters; an extremely low value of 0.013 RU was noted for the R1 station (Figure 4D). C4 intensities were strongly correlated with the intensities of the three humic-like components ($R^2 > 0.64$, $p < 0.001$, $n = 15$, Supplementary Figures S2D–F). The intensities of the three humic-like components (C1–C3) and C4 were positively correlated with DOC concentration ($R^2 = 0.38$–0.62, $p < 0.001$–0.02, $n = 14$), provided that the groundwater sample (G1) with abnormally low

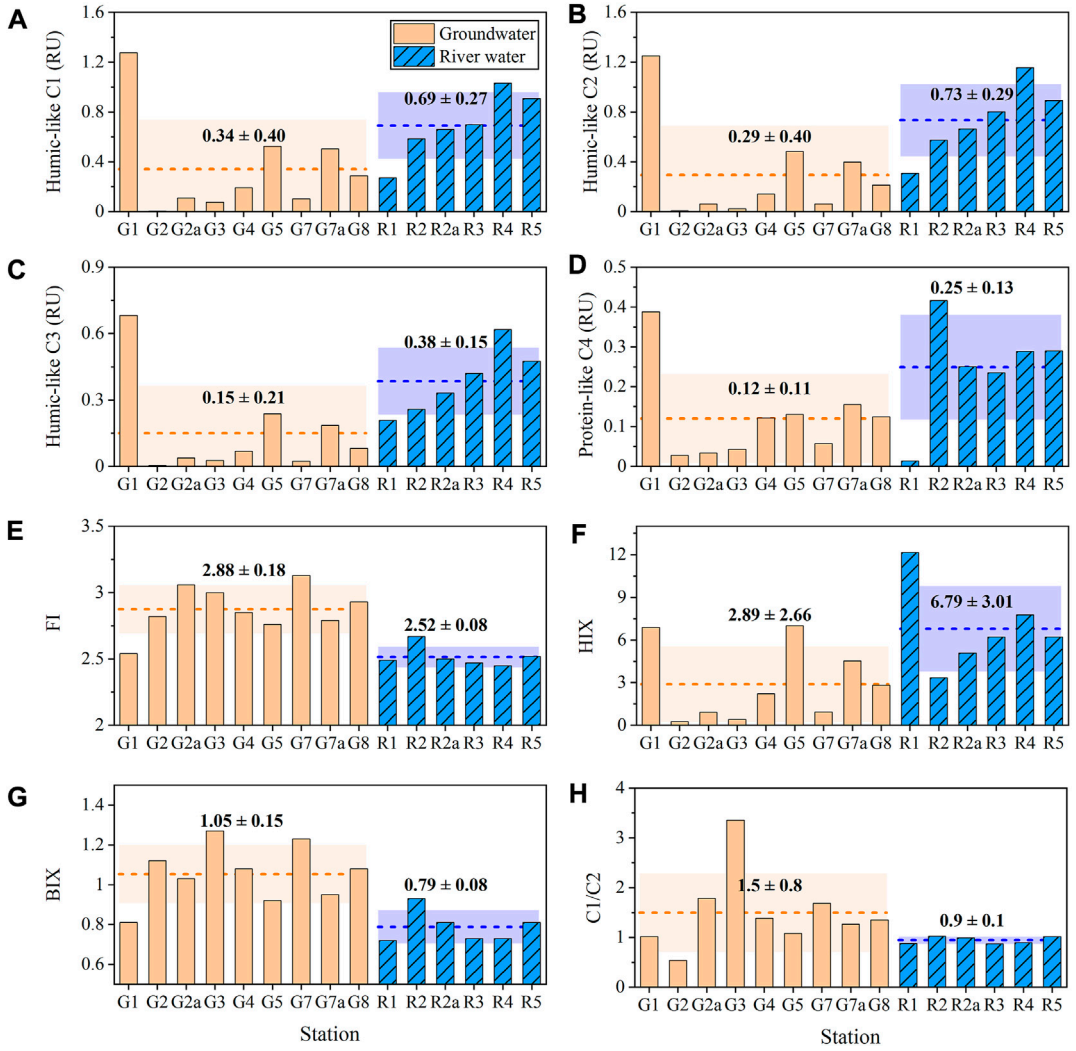

FIGURE 4
Distributions of **(A)** humic-like C1, **(B)** humic-like C2, **(C)** humic-like C3, **(D)** humic-like C4, **(E)** fluorescence index (FI), **(F)** humification index (HIX), **(G)** biological index (BIX) and **(H)** the ratio of C1 to C2 (C1/C2) in groundwater and river water samples. The dotted lines and shadows denote the average values and standard deviations, respectively.

DOC concentration was excluded from consideration (Supplementary Figures S3A–D). Similarly, the intensity of the four fluorescent components (C1–C4) was moderately related to a_{350} (R^2: 0.55–0.72, p: < 0.001–0.02, n = 14, Supplementary Figures S3E–H). Notably, the correlations between FDOM vs. DOC and FDOM vs. FDOM were absent when only groundwater samples were considered (Supplementary Figure S3). The intensity of C5 varied over the range of 0.007–0.35 RU and 0–0.05 RU in groundwater and river water samples, respectively. The average intensity of C5 in groundwaters (0.10 ± 0.11 RU) was ~30 times that in river waters (0.035 ± 0.019 RU). C5 intensity showed no correlations with DOC, a_{350}, and other FDOM components (p > 0.05) in groundwater and river water samples.

FI in groundwaters ranged from 2.5 to 3.1 (Figure 4E), with an average value of 2.9 ± 0.2, which was higher than that in river waters (2.5 ± 0.1, t-test, p < 0.001). BIX followed a similar trend, where a higher average value was noted for groundwater (1.05 ± 0.15) as compared to river water (0.79 ± 0.08, Figure 4G). On the contrary, HIX in groundwaters (2.9 ± 2.7) was significantly lower than that in river waters (6.8 ± 3.0, t-test, p < 0.001, Figure 4F). HIX was positively correlated to the intensities of humic-like components (R^2 = 0.39, p = 0.01, n = 15) but was negatively correlated with FI (R^2 = 0.64, p < 0.001, n = 15) and BIX (R^2 = 0.76, p = 0.01, n = 15, Supplementary Figures S4A–C). BIX showed a negative correlation with the intensities of humic-like components (R^2 = 0.62, p < 0.001, n = 15) and a strong positive correlation with FI (R^2 = 0.86, p < 0.001, n = 15) (Supplementary

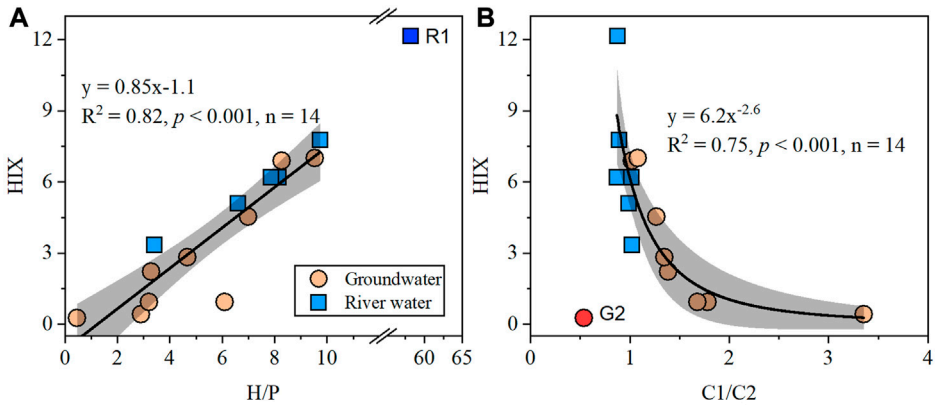

FIGURE 5
Relationships between **(A)** HIX and H/P and **(B)** HIX and C1/C2 in groundwater and river water samples. Sample R1 and G2 were excluded in the linear and exponential fittings (black solid lines), respectively. Gray shadows represent the 95% confidence bands for the fitting lines.

Figures S4D–E). The ratio of the two humic-like fluorescence components (C1/C2) ranged from 0.5 to 3.4 in groundwaters and from 0.9 to 1.0 in river water samples (Figure 4H), with a higher mean value in the former (*t*-test, $p < 0.001$). H/P ranged from 0.5 to 8.3 and 3.4 to 9.7 in groundwater and river water samples, respectively, except for an abrupt high value of 58.2 at the R1 station (Figure 5A). Generally, H/P was lower in groundwaters compared to that in river waters and was positively correlated with HIX ($R^2 = 0.82$, $p < 0.001$, $n = 14$, Figure 5A). Except for the G2 station, C1/C2 and HIX showed an exponential negatively correlation ($R^2 = 0.75$, $p < 0.001$, $n = 14$, Figure 5B).

4 Discussion

4.1 Interferences in colored dissolved organic matter absorption spectra of groundwater

The general exponential shape of CDOM absorption spectra in natural aquatic environments from inland watershed to the deep ocean (e.g., lake, river, estuary, coastal sea, and open ocean) has been known for decades (Jerlov, 1968; Stedmon et al., 2000; Nelson et al., 2010; Massicotte et al., 2017). Correspondingly, an exponential equation has been widely used to model CDOM absorption curves (Bricaud et al., 1981; Stedmon and Markager, 2001). The spectral slope derived from the fitting exponential equation became a good proxy for the average molecular weight of DOM, which was widely used to trace the DOM sources and associated biogeochemical processes (e.g., photochemical bleaching, humification process, diagenetic process) (Helms et al., 2013; Wang et al., 2017; Zhu et al., 2018; Yang et al., 2020). In this study, the absorption spectra of river water generally decrease with increasing wavelength, whilst the absorption curves of groundwater samples do not fully conform to the general exponential features of natural aquatic CDOM (Supplementary Figure S5). Instead, there is a strong absorption peak centered at 300 nm and abnormally high absorbance at a wavelength of <260 nm for all groundwater samples (Supplementary Figure S5). Previous studies have shown that nitrate concentration in groundwater was often several orders of magnitude higher than that in the surface natural water, which was attributed to strong microbial mineralization and anthropogenic discharge (Arslan et al., 2017). The mean nitrate concentration in 9 groundwater samples was up to 674 μmol L^{-1} (Table 1), which might result in considerable UV absorption superimposed on the CDOM absorption signal (Mack and Bolton, 1999). Here, we carried out a series of nitrate addition experiments (0, 200, 500, 1,000, 2000 μmol L^{-1}) in two groundwater (G2, G5) and two river water (R1, R2) samples. The absorption peak at 300 nm for all groundwater and river water samples was gradually highlighted with the increase of additional nitrate concentration (Supplementary Figure S6). Moreover, the influence of additional nitrates on the absorption spectra of groundwater and river water samples was restricted to a wavelength lower than 350 nm (Supplementary Figure S6), indicating that the selected a_{350} and $S_{350-400}$ could accurately evaluate the CDOM features in groundwater without being affected by the presence of high nitrate concentrations (Li and Hur, 2017).

During the additional experiments, the total absorption coefficients at 300 nm (a_{300}) showed a strong linear correlation with the total nitrate concentrations ($R^2 > 0.99$, $p < 0.001$, $n = 9$, Supplementary Figure S7). This provides powerful evidence that a high concentration of nitrate (>100 μmol L^{-1}) was the primary factor responsible for the occurrence of the visible absorption peaks at 300 nm in all

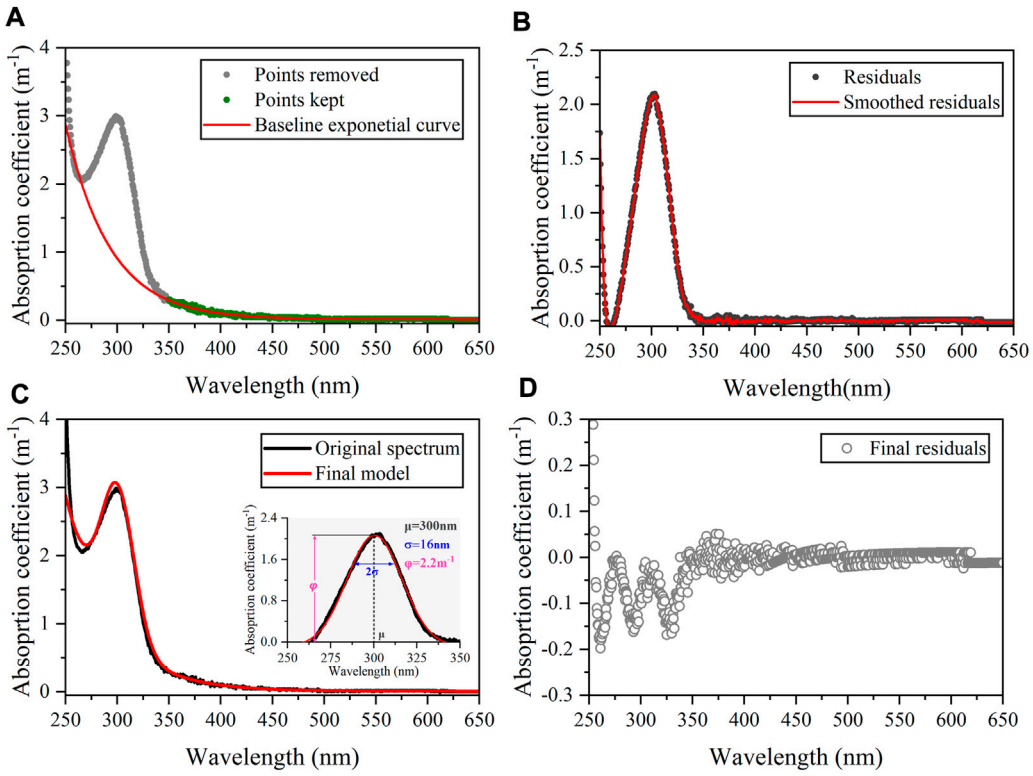

FIGURE 6
Schema of the modeling framework illustrating the fitting process on groundwater absorption curve using an exponential-Gaussian equation (taking G2 station as an example). **(A)** Result of the baseline exponential fitting process. Gray points have been discarded to calculate the baseline exponential curve. **(B)** Residual plot of the baseline exponential model (observed data−fitted data). **(C)** The estimated Gaussian parameters and final exponential-Gaussian model result **(D)** Final residuals from the estimated spectrum (observed data−fitted data).

groundwater samples (Supplementary Figure S2A). The intercepts of the above linear regressions represent the absorption signal of groundwater samples excluding the contribution of nitrate (Supplementary Figure S7). Aside from nitrate, ferric iron and nitrite are also absorbers of UV-Visible radiation (Mack and Bolton, 1999; Xiao et al., 2013) and thus may interfere with CDOM absorbance at elevated concentrations. Yet the total dissolved Fe and nitrite concentrations are <0.8 μmol L^{-1} and <26 μmol L^{-1} in groundwater and river water samples (Table 1), respectively, making them unlikely to significantly affect the absorption spectra and the absorbance-based $SUVA_{350}$ values in this study (Hansen et al., 2016).

4.2 Mathematical decomposition of absorption curves

After depicting the nitrate absorption curve and confirming its interference in absorption spectra, an exponential-Gaussian approach could be applied to distinguish the absorption of CDOM and nitrate in all groundwater and river water samples (Massicotte and Markager, 2016). Firstly, the absorption spectra between 350 nm and 650 nm were demonstrated to be attributed to the CDOM signal (Supplementary Figure S6) and were fitted using the general exponential equation (Eq. 2, Figure 6A). Next, the residuals of the baseline exponential model for the whole spectrum (250–650 nm) were smoothed using a Savitsky–Golay method to remove potential noise in the data (Figure 6B). The smoothed residuals were then modeled using the following Gaussian curve:

$$f(x, \varphi, \mu, \sigma) = \varphi e^{\frac{-(\lambda-\mu)^2}{2\sigma^2}} \quad (4)$$

where σ is the standard deviation (nm) controlling the width of the curve, φ is the height of the curve peak (m^{-1}, $\varphi = \frac{1}{\sigma\sqrt{2\Pi}}$) and μ is the position of the center of the peak (nm). Here, the μ is 300 nm for all curves according to the validation of the nitrate addition experiment, and the φ was estimated as the residual at 300 nm for each curve (Figure 6C). Finally, the complete spectra for groundwater and river water samples were fitted using an exponential equation plus one Gaussian component (Figure 6D):

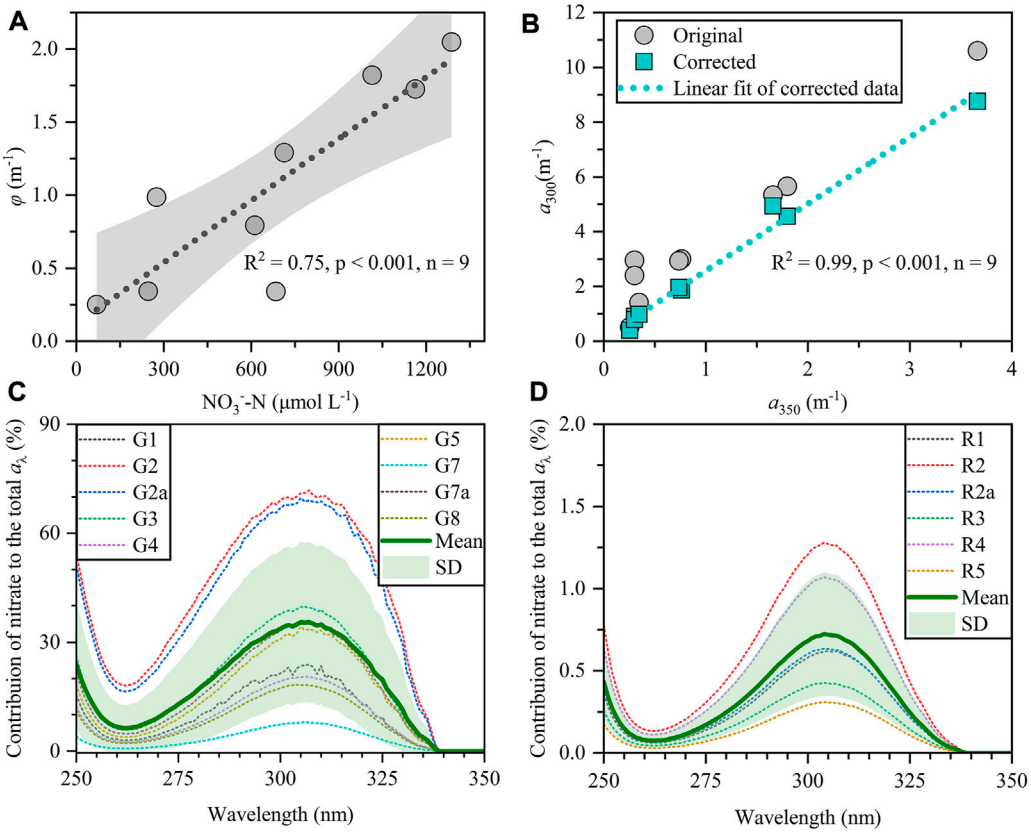

FIGURE 7
Relationships **(A)** between φ values and nitrate concentrations and **(B)** between original and model-corrected absorption coefficients at 300 nm and 350 nm in groundwater samples, and the contribution of nitrate to the total absorption coefficient($a\lambda$) in **(C)** groundwater and **(D)** river water samples. Green solid lines and bands represent the mean values and standard deviations (SD), respectively.

$$a_\lambda = a_{\lambda_0} e^{-s(\lambda-\lambda_0)} + \varphi e^{\frac{-(\lambda-\mu)^2}{2\sigma^2}} + \varepsilon \quad (5)$$

where e is the final residual representing the variability not accounted for by the model. The estimated φ values were positively correlated with nitrate concentrations in groundwater samples (R^2 = 0.75, p < 0.001, n = 9, Figure 7A). Furthermore, a strong linear relationship between the original a_{350} and corrected a_{300} in groundwater samples occurred when the Gaussian component was removed (R^2 = 0.99, p < 0.001, n = 9, Figure 7B), which follows the common feature that CDOM absorption coefficients at two wavelengths (300 vs. 350 nm) show synchronous changes at the land-sea interface (Massicotte et al., 2017; Li et al., 2019). These results prove that the exponential-Gaussian equation is sufficient to distinguish CDOM and nitrate absorption signals throughout the natural or engineered systems with the advantages of simplicity, rapidity, and low cost, which has good potential in the simultaneous monitoring of aquatic carbon and water quality.

The mathematical method showed that the contributions of nitrate to the total absorbance of groundwater were apparent. It showed a maximum at the wavelength of ~300 nm and <250 nm and a lower value near the wavelength of ~260 nm (Figure 7C). In terms of several wavelengths commonly used to quantify CDOM (Massicotte et al., 2017), the absorption of nitrate accounted for 13% ± 12% (254 nm), 17% ± 14% (280 nm), 34% ± 22% (300 nm), 20% ± 17% (325 nm) of the total absorption in nine groundwater samples (Figure 7C), respectively, demonstrating the considerable interference of high concentration nitrate on groundwater CDOM absorption spectra in western Guangdong. In sharp contrast, the average contribution of nitrate to the absorbance for six river water samples was less than 1% over the whole wavelength range (Figure 7D). Generally, the *in situ* biological productions of riverine CDOM are concomitant with the consumption of nitrate. The aphotic groundwater CDOM could be consumed as the substrate of microbes (McDonough et al., 2022), whereas various geogenic interactions and anthropogenic pollutions lead to the rapid accumulation of nitrate in groundwaters (Huno et al., 2018). As a result, the ratio of CDOM to nitrate inventory enhances in the river water but declines in the groundwater,

which is the predominated factor for the emergence of distinctive absorption curves in two types of natural fresh waters.

4.3 Factors affecting the sources, compositions, and levels of DOM in groundwaters and river waters

Previous studies showed that the optical parameters could provide valuable information on the source and composition of DOM in aquatic environments (Baker, 2001; Chen et al., 2010; Derrien et al., 2017; Li and Hur, 2017; D'Andrilli et al., 2022). The relatively high contribution of humic-like components to total FDOM fluorescence was found in both the groundwater (77 ± 18%) and river water samples (88 ± 7%), suggesting that the highly reworked humic-like molecules dominate the riverine and groundwater DOM pool (Figure 5A). Higher FI (2.88 ± 0.18), BIX (1.05 ± 0.15) and C1/C2 (1.50 ± 0.8) values observed in groundwater (Figures 4E,G,H) further indicate that the humic-like components in groundwater were mainly produced by the recent *in situ* microbial activity (Cory and Mcknight, 2005; Huguet et al., 2009). In contrast, the direct input of terrestrial soil humus through infiltration had a considerable contribution to the humic-like DOM in river water. It was consistent with the lower molecular weight and aromaticity of groundwater DOM, as supported by higher $S_{350-400}$ and lower $SUVA_{350}$ values in groundwaters (Figures 2C,D). We also found a strong linear correlation between DOC and a_{350} (Supplementary Figure S1A) but an absence of a link between a_{350} and humic-like FDOM in groundwater (Supplementary Figure S3). It seemed to indicate that groundwater CDOM could serve as the labile substrate for microbial activity, which differed from the general rule that CDOM shares a similar distribution pattern to humic-like FDOM in the surface natural aquatic environment (Guo et al., 2014). A possible explanation from a case in the deep Mediterranean Sea where was that microbes could consume relatively refractory CDOM when the DOC is insufficient and the environment is warm (Catalá et al., 2018). However, the linear correlations among DOC, CDOM, and FDOM in river water samples (Supplementary Figure S3) supported that their distributions were mainly regulated by the same process (i.e., the terrestrial input). This conclusion sounds to be reasonable because the high precipitation occurred during the sampling period (315 mm/month, https://www.ncei.noaa.gov/) which could intensify the soil erosion and induce an enrichment of terrigenous DOM in river water (Qu et al., 2020). On the other hand, the residence time of groundwater was generally longer than surface river water (Downing and Striegl, 2018), permitting a stronger microbial reworking of DOM and lower DOC inventory preserved in the aquifer (Figure 2A).

In this study, the DOC concentration of groundwater in western Guangdong (94 ± 62 μmol L^{-1}) was close to the lower limit of the range of reported global groundwater DOC concentration (McDonough et al., 2022). Previous studies have confirmed that the variations of aquifer depth (age), land use, precipitation, and water chemical environment (e.g., ionic strength, redox condition) are key factors shaping the levels of DOM in the groundwater system (McDonough et al., 2020a; McDonough et al., 2020b; Moore and Joye, 2021). Groundwater samples in this study were collected from wells for domestic use and should represent shallow aquifers with water tables of <3 m. Generally, shallow groundwater with a longer residence time and larger aquifer age tends to have a lower DOC concentration than surface water as a result of enhanced removal pathways such as oxidation processes, biodegradation, and adsorption to soil and aquifer mineral surfaces (Shen, 1999; Downing and Striegl, 2018). In addition, the sampling region was mostly covered by natural and agricultural land that receives lower amounts of organic contaminants from human activities than the region within urban land use (Figure 1). It may be a critical factor responsible for the low DOC concentration in western Guangdong compared to that in the region within urban land use (McDonough et al., 2022). Another important factor is reflected in the enhanced dilution effect owing to high precipitation in the study area (~1800 mm/yr, Chen et al., 2021), whereby accumulated soil DOM infiltrates the aquifer during initial rainfall and is later diluted by additional rainfall (McDonough et al., 2020a). Accordingly, we speculated that the comparable but low concentrations of groundwater DOC observed in western Guangdong between July 2021 and April 2012 (94 ± 62 vs. 97 ± 40 μmol L^{-1}, Dai et al., 2021) could be closely associated with the equivalent but high precipitation over the sampling periods (315 vs. 343 mm/month, https://www.ncei.noaa.gov/). Although parameters related to water chemical conditions were not considered in this study, we also found the implication between the groundwater DOM and water chemistry in western Guangdong by running a comparison with other data along the global coast (Figure 8). The groundwater DOC concentration in western Guangdong was only higher than that on the coast of Taiwan Island (45 ± 20 μmol L^{-1}, Yang et al., 2015), the western coast of South Korea (72 ± 20 μmol L^{-1}, Kim et al., 2012). It was slightly lower than that on the coast of Hainan Island (114 ± 112 μmol L^{-1}, Wang et al., 2018), the southeastern coast of South Korea (139 ± 23 μmol L^{-1}, Oh et al., 2017), and Chongming Island (212 ± 170 μmol L^{-1}, He et al., 2022), but significantly lower than that in southern Guangxi (732–1,184 μmol L^{-1}, Chen et al., 2018), America (196–1,020 μmol L^{-1}, Goodridge, 2018; Pain et al., 2019; Qi et al., 2018; Porubsky et al., 2014; Suryaputra et al., 2015), Australia (369–882 μmol L^{-1}, Maher et al., 2013; Stewart et al., 2015; Webb et al., 2019), Indian islands (318 μmol L^{-1}, Tedetti et al., 2011) and Europe (334–483 μmol L^{-1}, Szymczycha et al., 2014; Ibánhez et al., 2021). Overall, the groundwater with low DOC concentration collected in western Guangdong was freshwater (salinity = 0, Table 1), while the majority of the

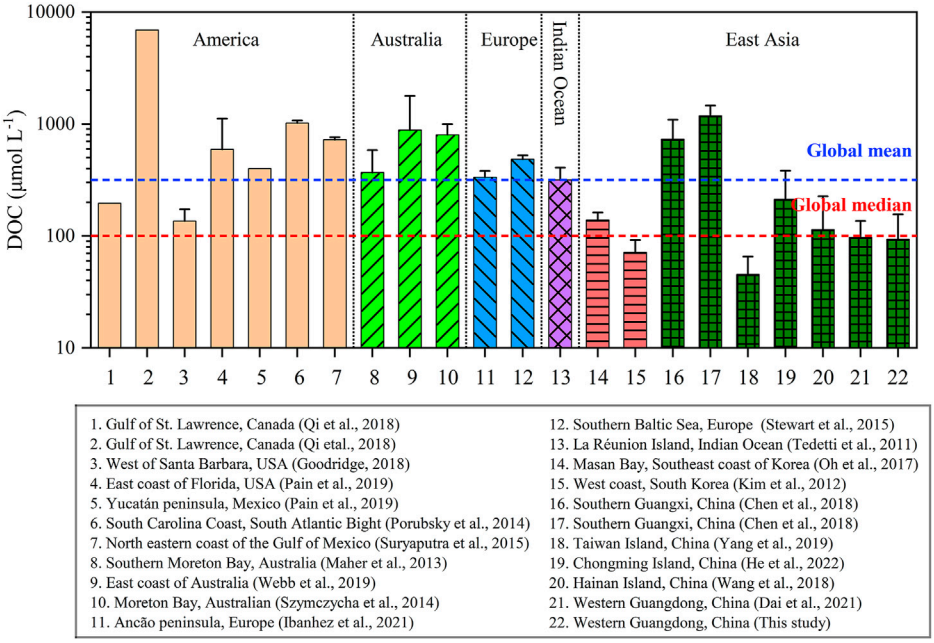

FIGURE 8
Histogram showing groundwater DOC concentrations in global coast regions. Error bars represent the standard deviations of multiple data for individual columns. Red and blue dashed lines indicate the global median and mean values of groundwater DOC concentrations (n = 9,404), respectively, presented by McDonough et al. (2020a).

other coastal groundwaters with high DOC levels were significantly affected by seawater intrusion and were termed recirculated seawater (Figure 8). The seawater intrusion could mobilize surface-bond ions and organic matter absorbed onto sediment and further accelerate the degradation of organic matter *via* anaerobic metabolism, which could lead to increased DOC concentration in salty coastal groundwater (Moore and Joye, 2021).

Globally, the level of DOC and CDOM among the 52 rivers around the world varied over a wide range of 28–868 μmol L^{-1} and 0.15–23 m^{-1}, respectively (Supplementary Table S1). High values were found in the pan-Arctic great rivers surrounded by soil with high inventories of organic matter (Stedmon et al., 2011), the tropical large rivers concomitant with high watershed vegetation productivities (López et al., 2012; Lambert et al., 2015; Raymond and Spencer, 2015; Valerio et al., 2018) and some populated rivers with high loading of anthropogenic pollutants (Spencer et al., 2013; Yang et al., 2013). Correspondingly, low DOC and CDOM concentrations are often observed in natural rivers with little vegetation cover and such as subtropical rivers on the Chinese mainland and mountain rivers on Taiwan Island (Yang et al., 2013; Guo et al., 2014; Li et al., 2019). Here, the concentrations of DOC and CDOM in the small tropical rivers of western Guangdong were high–moderate among the global 52 rivers and were comparable to those in large tropical rivers (e.g., Amazon and Orinoco Rivers). These tropical rivers still shared an equivalent ratio of a_{350} to DOC, which may indicate that the small tropical rivers in western Guangdong received a large quantity of highly aromatic DOM as a result of a high cover of dense vegetation (Lambert et al., 2015). The ratio of a_{350} to DOC in river waters of western Guangdong was only lower than that in United States rivers (Figures 9A,B) but larger than those in other categories such as pan-Arctic rivers, small mountains, and populated rivers in Taiwan Island and Chinese mainland rivers (Figure c–f). It broke the previous result based on limited data that temperate rivers had a moderate ratio of a_{350} to DOC (Lambert et al., 2015). Many factors such as climate zone, land cover, watershed morphology, climate change, and human-induced perturbation may regulate this ratio as well as the composition of riverine DOM (Guo et al., 2014; Lambert et al., 2015; Qu et al., 2020, 2022), thereby exerting a potentially important impact on the local coastal ecosystem.

4.4 The export flux of DOM by fresh groundwater discharge and river runoff

Previous studies reported that the fresh groundwater discharge flux in western Guangdong was up to 4.74 × 10^{10} m^3 yr^{-1} (Zhang and Li, 2005; Tan et al., 2018), amounting to more than 2 times the total river runoff in this region (1.84 × 10^{10} m^3 yr^{-1}). Even so, the export fluxes of DOC and FDOM by

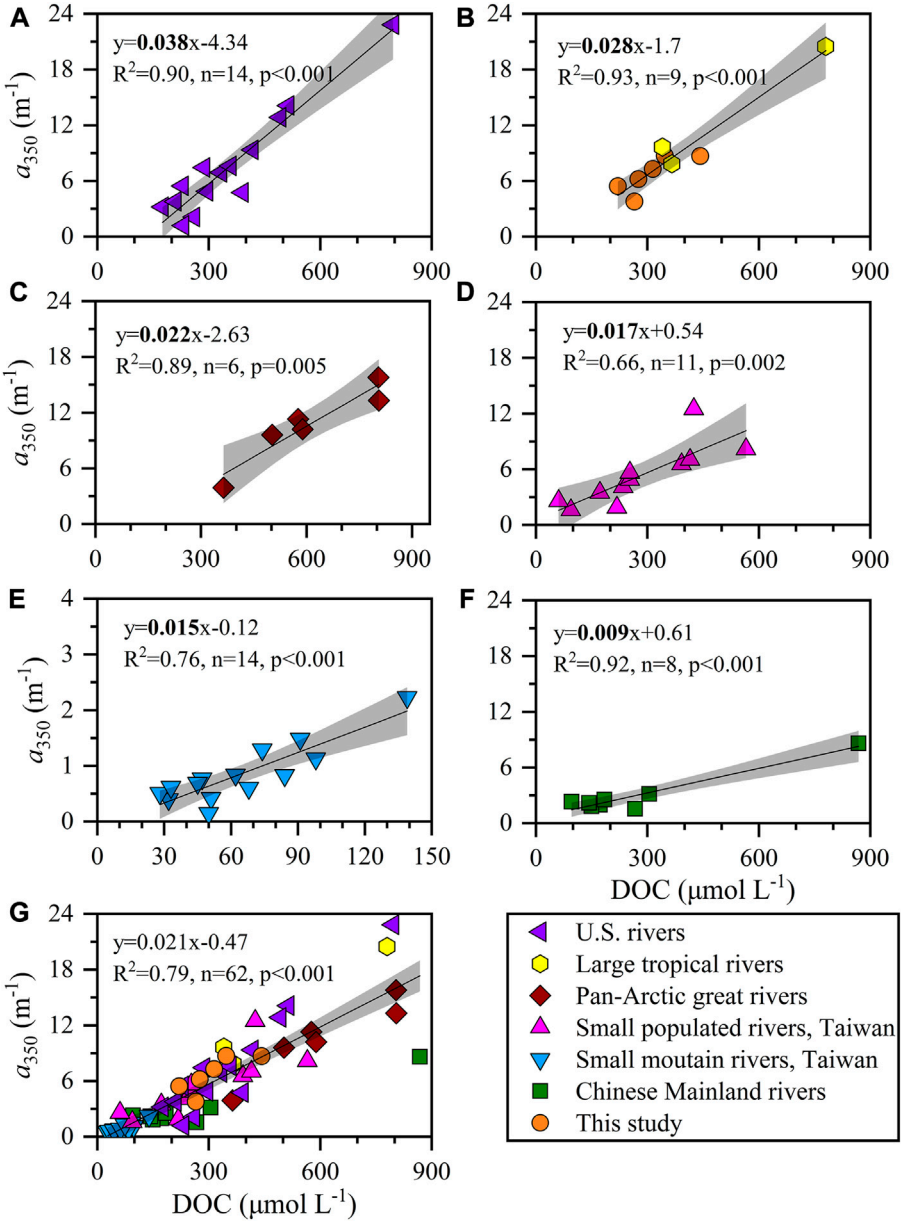

FIGURE 9
The correlations between DOC and a_{350} in **(A)** United States rivers, **(B)** our study and tropical large rivers, **(C)** pan-Arctic great rivers, **(D)** small populated rivers, Taiwan Island, **(E)** small mountain rivers, Taiwan Island, **(F)** Chinese Mainland rivers and **(G)** a total of 52 rivers in the globe. Blank lines and gray shadows represent the linear fits and confident bands (95%), respectively. Data are listed in Supplementary Table S1.

fresh groundwater discharge were comparable to those by river runoff (Table 2) due to the huge difference in DOM levels between the groundwater and surface river systems (Figures 2, 4). The CDOM export flux by fresh groundwater discharge was even 40% of that by river runoff in western Guangdong (Table 2). By comparison with the river with the highest flow around the South China Sea, the Peral River, the fluxes of water, DOC, and CDOM by groundwater discharge in western Guangdong to the South China Sea accounted for 16%–18% of the fluxes by the Pearl River runoff (Table 2, Li et al., 2019). Globally, the paired data of DOC and CDOM in the groundwater environment are quite lacking compared with the single study of groundwater DOC (McDonough et al., 2020a). Using the slope of correlation between a_{350} and DOC in the groundwater (0.016 ± 0.003,

TABLE 2 The export fluxes of water, DOC, CDOM, and FDOM *via* fresh groundwater discharge and river runoff in western Guangdong.

	Water flux	DOC flux	CDOM flux (a_{350})	Humic-like C1 flux	Humic-like C2 flux	Humic-like C3 flux	Protein-like C4 flux
	10^9 m^3 yr^{-1}	10^9 g C yr^{-1}	10^9 m^2 yr^{-1}	10^9 RU m^3 yr^{-1}	10^9 RU m^3 yr^{-1}	10^9 RU m^3 yr^{-1}	10^9 RU m^3 yr^{-1}
Jian River	8.98	41 ± 9.7	72 ± 8.9	8.7 ± 0.8	9.2 ± 1.7	4.9 ± 0.9	2.6 ± 0.01
Moyang River	8.59	22.8	46.7	5.0	4.9	2.2	3.6
Rudong River	0.86	3.6	7.5	0.6	0.7	0.36	0.2
Total	18.4	67 ± 9.7	126 ± 8.9	14 ± 0.8	15 ± 1.7	7.5 ± 0.9	6.4 ± 0.01
Groundwater	47.4	53 ± 35	52 ± 53.5	16 ± 19	14 ± 19	7.1 ± 10	5.7 ± 5.3

Supplementary Figure S1), the global median and mean groundwater concentrations (100 and 317 μmol L^{-1}, McDonough et al., 2020a) and the water flux to the ocean *via* SGD (2.2–2.4 × 10^{12} m^3 yr^{-1}, Zektser et al., 2007), these values represent 3.5–12.2 × 10^{12} m^2 yr^{-1} of groundwater CDOM (a_{350}-based) exported to oceans from SGD annually. A total of 52 rivers summarized in this study with respect to discharge contribute ~39% of the total annual global discharge and were located across the major continents and climatic zones (Supplementary Table S1). In this sense, the correlation between a_{350} and DOC could reflect the general feature of global rivers. The global CDOM flux (a_{350}-based) by river runoff can be estimated at 4.3 ± 0.3 × 10^{14} m^2 yr^{-1} based on the slope of the above correlation (0.021 ± 0.001, Figure 9G), and the global riverine DOC flux of 250 Tg C yr^{-1} (Raymond and Spencer, 2015). Owing to its high sensitivity to photochemical and/or biological degradations (Fichot and Benner, 2014; McDonough et al., 2022), the impact of exported DOM by SGD and river runoff on coastal carbon budget and ecosystem is significant under the background of the changing climate and intensified human activities.

5 Conclusion

The first comprehensive investigation of DOC, CDOM, and FDOM in the groundwater and river water from western Guangdong reveals the distinct sources, levels, composition, and export fluxes of DOM to these aquatic reservoirs. High concentrations of nitrate, rather than nitrite or dissolved iron, lead to the non-exponential absorption spectra observed in groundwater but were restricted to the wavelength of <350 nm. The nitrate contribution to total absorption was apparent in groundwater but was small in river water, which should be considered in the future characterization of CDOM. The successful application of an exponential-gaussian equation on the precise separation of CDOM and nitrate absorption signals highlights an important experimental prospect for the synchronous monitoring of groundwater organic matter and nutrients.

Five PARAFAC components were identified in groundwater and river water samples, including three humic-like and two protein-like fluorescence components. Both groundwater and river water samples were dominated by humic-like components, accounting for ~87% of the total fluorescence intensity. The DOC concentration, a_{350}, and FDOM intensity in groundwater samples were significantly lower than those in river water samples. Moreover, groundwater DOM had higher $S_{350–400}$, FI, BIX, and C1/C2, but featured lower HIX and $SUVA_{350}$, suggesting that it mainly originated from microbial activities; terrestrial input had a considerable contribution to river water DOM. In the global context, groundwater DOC concentration in western Guangdong was low–moderate, while river water DOC and a_{350} concentrations were high–moderate. Several factors (e.g., precipitation, land use, water chemistry, and watershed vegetation productivity) functioning in concert may lead to this phenomenon.

The fluxes of DOC and CDOM by fresh groundwater discharge in western Guangdong were found to be comparable in magnitude to those *via* the total runoff of rivers in the same region and the adjacent Pearl River. These observations demonstrate that groundwater discharge in western Guangdong is an important source of allochthonous DOM to the northern shelf of the South China Sea. The linear relationships between CDOM and DOC were pronounced in groundwater and river water samples; they showed large variability among different river categories, which is likely to be related to complex factors, such as climatic zone, land use, and human activities. Based on the slopes and the reported data on water fluxes and DOC levels, the global CDOM fluxes *via* groundwater discharge and river runoff are reported. More case studies are needed in the future to reduce the bias in calculating CDOM flux and deepen the understanding of their impact on the coastal carbon cycle.

Data availability statement

The original contributions presented in the study are included in the article/Supplementary Material, further inquiries can be directed to the corresponding authors.

Author contributions

CW and GJ designed the study. CW and JG participated in field sampling. YL and XH performed sample analysis. CW carried out data processing. CW, XH, and GJ prepared the manuscript. All authors listed have made a substantial, direct, and intellectual contribution to the work, and approved it for publication.

Funding

This work is supported by the program for scientific research start-up funds of Guangdong Ocean University (060302032009), the open grant from Guangxi Key Laboratory of Beibu Gulf Marine Resources, Environment and Sustainable Development (MRESD-2022-B01), and the Guangdong Province First-class Discipline Plan (CYL231420003).

Acknowledgments

The authors thank Jiacheng Li for his help in the sample collection. Xuan Lu is also thanked for his assistance in DOC analysis. We would like to thank Qun Xie at the Analytical and Testing Center of Guangdong Ocean University for her assistance with the analysis of iron concentration. We gratefully thank the three reviewers for their careful reviews, insightful comments, and valuable suggestions.

Conflict of interest

The authors declare that the research was conducted in the absence of any commercial or financial relationships that could be construed as a potential conflict of interest.

Publisher's note

All claims expressed in this article are solely those of the authors and do not necessarily represent those of their affiliated organizations, or those of the publisher, the editors and the reviewers. Any product that may be evaluated in this article, or claim that may be made by its manufacturer, is not guaranteed or endorsed by the publisher.

Supplementary material

The Supplementary Material for this article can be found online at: https://www.frontiersin.org/articles/10.3389/fenvs.2022.995190/full#supplementary-material

References

Arslan, H., Turan, N. A., Demir, Y., Gungor, A., and Cemek, B. (2017). Assessment of spatial and seasonal changes in groundwater nitrate pollution of agricultural lands through ordinary and indicator kriging techniques. *Archives Agron. Soil Sci.* 63, 907–917. doi:10.1080/03650340.2016.1249472

Baker, A. (2001). Fluorescence excitation-emission matrix characterization of some sewage-impacted rivers. *Environ. Sci. Technol.* 35, 948–953. doi:10.1021/es000177t

Baker, M. A., Valett, H. M., and Dahm, C. N. (2000). Organic carbon supply and metabolism in a shallow groundwater ecosystem. *Ecology* 81, 3133–3148. doi:10.1890/0012-9658(2000)081[3133:ocsami]2.0.co;2

Bricaud, A., Morel, A., and Prieur, L. (1981). Absorption by dissolved organic matter of the sea (yellow substance) in the UV and visible domains1. *Limnol. Oceanogr.* 26, 43–53. doi:10.4319/lo.1981.26.1.0043

Carlson, C. A., and Hansell, D. A. (2015). "Chapter 3 - DOM sources, sinks, reactivity, and budgets," in *Biogeochemistry of marine dissolved organic matter*. Editors D. A. Hansell and C. A. Carlson. Second Edition (Boston: Academic Press), 65–126.

Carlson, K. M., and Wiegner, T. N. (2016). Effects of submarine groundwater discharge on bacterial growth efficiency in coastal Hawaiian waters. *Aquat. Microb. Ecol.* 77, 167–181. doi:10.3354/ame01797

Catalá, T. S., Martínez–Pérez, A. M., Nieto-Cid, M., Álvarez, M., Otero, J., Emelianov, M., et al. (2018). Dissolved organic matter (DOM) in the open Mediterranean Sea. I. Basin-Wide distribution and drivers of chromophoric DOM. *Prog. Oceanogr.* 165, 35–51. doi:10.1016/j.pocean.2018.05.002

Catalá, T. S., Reche, I., Fuentes-Lema, A., Romera-Castillo, C., Nieto-Cid, M., Ortega-Retuerta, E., et al. (2015). Turnover time of fluorescent dissolved organic matter in the dark global ocean. *Nat. Commun.* 6, 5986. doi:10.1038/ncomms6986

Chen, F., Huang, C., Lao, Q., Zhang, S., Chen, C., Zhou, X., et al. (2021). Typhoon control of precipitation dual isotopes in Southern China and its palaeoenvironmental implications. *Geophys. Res. Atmos.* 126, e2020JD034336. doi:10.1029/2020JD034336

Chen, M., Price, R. M., Yamashita, Y., and Jaffe, R. (2010). Comparative study of dissolved organic matter from groundwater and surface water in the Florida coastal Everglades using multi-dimensional spectrofluorometry combined with multivariate statistics. *Appl. Geochem.* 25, 872–880. doi:10.1016/j.apgeochem.2010.03.005

Chen, X., Zhang, F., Lao, Y., Wang, X., Du, J., and Santos, I. R. (2018). Submarine groundwater discharge-derived carbon fluxes in mangroves: An important component of blue carbon budgets? *J. Geophys. Res. Oceans* 123, 6962–6979. doi:10.1029/2018jc014448

Coble, P. G. (1996). Characterization of marine and terrestrial DOM in seawater using excitation emission matrix spectroscopy. *Mar. Chem.* 51, 325–346. doi:10.1016/0304-4203(95)00062-3

Collins, M., Knutti, R., Arblaster, J., Dufresne, J.-L., Fichefet, T., Friedlingstein, P., et al. (2013). "Long-term climate change: Projections, commitments and irreversibility," in *Climate change 2013: The physical science basis. Contribution of working group I to the fifth assessment report of the intergovernmental panel on climate change*. Editors T. F. Stocker, D. Qin, G.-K. Plattner, M. Tignor, S. K. Allen, J. Boschung, et al. (Cambridge, United Kingdom and New York, NY, USA: Cambridge University Press).

Cory, R. M., and Mcknight, D. M. (2005). Fluorescence spectroscopy reveals ubiquitous presence of oxidized and reduced quinones in dissolved organic matter. *Environ. Sci. Technol.* 39, 8142–8149. doi:10.1021/es0506962

Dai, G., Wang, G., Li, Q., Tan, E., and Dai, M. (2021). Submarine groundwater discharge on the Western shelf of the northern South China Sea influenced by the Pearl River plume and upwelling. *J. Geophys. Res. Oceans* 126, e2020JC016859. doi:10.1029/2020JC016859

D'andrilli, J., Silverman, V., Buckley, S., and Rosario-Ortiz, F. L. (2022). Inferring ecosystem function from dissolved organic matter optical properties: A critical review. *Environ. Sci. Technol.* 56, 11146–11161. doi:10.1021/acs.est.2c04240

Derrien, M., Yang, L., and Hur, J. (2017). Lipid biomarkers and spectroscopic indices for identifying organic matter sources in aquatic environments: A review. *Water Res.* 112, 58–71. doi:10.1016/j.watres.2017.01.023

Donn, M. J., and Barron, O. V. (2013). Biogeochemical processes in the groundwater discharge zone of urban streams. *Biogeochemistry* 115, 267–286. doi:10.1007/s10533-013-9833-5

Downing, J. A., and Striegl, R. G. (2018). Size, age, renewal, and discharge of groundwater carbon. *Inland Waters* 8, 122–127. doi:10.1080/20442041.2017.1412918

Ferguson, G., Mcintosh, J. C., Warr, O., Sherwood Lollar, B., Ballentine, C. J., Famiglietti, J. S., et al. (2021). Crustal groundwater volumes greater than previously thought. *Geophys. Res. Lett.* 48, e2021GL093549. doi:10.1029/2021GL093549

Fichot, C. G., and Benner, R. (2014). The fate of terrigenous dissolved organic carbon in a river-influenced ocean margin. *Glob. Biogeochem. Cycles* 28, 300–318. doi:10.1002/2013gb004670

Goodridge, B. M. (2018). The influence of submarine groundwater discharge on nearshore marine dissolved organic carbon reactivity, concentration dynamics, and offshore export. *Geochimica Cosmochimica Acta* 241, 108–119. doi:10.1016/j.gca.2018.08.040

Guo, W., Yang, L., Hong, H., Stedmon, C. A., Wang, F., Xu, J., et al. (2011). Assessing the dynamics of chromophoric dissolved organic matter in a subtropical estuary using parallel factor analysis. *Mar. Chem.* 124, 125–133. doi:10.1016/j.marchem.2011.01.003

Guo, W., Yang, L., Zhai, W., Chen, W., Osburn, C. L., Huang, X., et al. (2014). Runoff-mediated seasonal oscillation in the dynamics of dissolved organic matter in different branches of a large bifurcated estuaryThe Changjiang Estuary. *J. Geophys. Res. Biogeosci.* 119, 776–793. doi:10.1002/2013jg002540

Hansell, D. A., Carlson, C. A., Repeta, D. J., and Schlitzer, R. (2009). Dissolved organic matter in the ocean: A controversy stimulates new insights. *Oceanogr. Wash. D. C).* 22, 202–211. doi:10.5670/oceanog.2009.109

Hansen, A. M., Kraus, T. E. C., Pellerin, B. A., Fleck, J. A., Downing, B. D., and Bergamaschi, B. A. (2016). Optical properties of dissolved organic matter (DOM): Effects of biological and photolytic degradation. *Limnol. Oceanogr.* 61, 1015–1032. doi:10.1002/lno.10270

He, T., Zhang, F., Wang, Y., Chen, X., and Du, J. (2022). Characterization of dissolved organic matter in submarine groundwater from a salt marsh in Chongming Island, China. *J. Oceanol. Limnol.* 40, 128–141. doi:10.1007/s00343-021-0296-6

Helms, J. R., Stubbins, A., Perdue, E. M., Green, N. W., Chen, H., and Mopper, K. (2013). Photochemical bleaching of oceanic dissolved organic matter and its effect on absorption spectral slope and fluorescence. *Mar. Chem.* 155, 81–91. doi:10.1016/j.marchem.2013.05.015

Helms, J. R., Stubbins, A., Ritchie, J. D., Minor, E. C., Kieber, D. J., and Mopper, K. (2008). Absorption spectral slopes and slope ratios as indicators of molecular weight, source, and photobleaching of chromophoric dissolved organic matter. *Limnol. Oceanogr.* 53, 955–969. doi:10.4319/lo.2008.53.3.0955

Huguet, A., Vacher, L., Relexans, S., Saubusse, S., Froidefond, J. M., and Parlanti, E. (2009). Properties of fluorescent dissolved organic matter in the Gironde Estuary. *Org. Geochem.* 40, 706–719. doi:10.1016/j.orggeochem.2009.03.002

Huno, S. K. M., Rene, E. R., Van Hullebusch, E. D., and Annachhatre, A. P. (2018). Nitrate removal from groundwater: A review of natural and engineered processes. *J. Water Supply Res. Technology-Aqua* 67, 885–902. doi:10.2166/aqua.2018.194

Ibánhez, J. S. P., Antón Álvarez-Salgado, X., and Rocha, C. (2021). Does nitrate enrichment accelerate organic matter turnover in subterranean estuaries? *Front. Mar. Sci.* 8. doi:10.3389/fmars.2021.661201

Jerlov, N. (1968). *Optical oceanography*. New York: Elsevier Publishing Company, 194.

Kalbitz, K., Solinger, S., Park, J. H., Michalzik, B., and Matzner, E. (2000). Controls on the dynamics of dissolved organic matter in soils: A review. *Soil Sci.* 165, 277–304. doi:10.1097/00010694-200004000-00001

Kim, J., and Kim, G. (2017). Inputs of humic fluorescent dissolved organic matter via submarine groundwater discharge to coastal waters off a volcanic island (Jeju, Korea). *Sci. Rep.* 7, 7921. doi:10.1038/s41598-017-08518-5

Kim, T.-H., Waska, H., Kwon, E., Suryaputra, I. G. N., and Kim, G. (2012). Production, degradation, and flux of dissolved organic matter in the subterranean estuary of a large tidal flat. *Mar. Chem.* 142, 1–10. doi:10.1016/j.marchem.2012.08.002

Kothawala, D. N., Murphy, K. R., Stedmon, C. A., Weyhenmeyer, G. A., and Tranvik, L. J. (2013). Inner filter correction of dissolved organic matter fluorescence. *Limnol. Oceanogr. Methods* 11, 616–630. doi:10.4319/lom.2013.11.616

Kowalczuk, P., Tilstone, G. H., Zabłocka, M., Röttgers, R., and Thomas, R. (2013). Composition of dissolved organic matter along an Atlantic Meridional Transect from fluorescence spectroscopy and Parallel Factor Analysis. *Mar. Chem.* 157, 170–184. doi:10.1016/j.marchem.2013.10.004

Kwon, E. Y., Kim, G., Primeau, F., Moore, W. S., Cho, H.-M., Devries, T., et al. (2014). Global estimate of submarine groundwater discharge based on an observationally constrained radium isotope model. *Geophys. Res. Lett.* 41, 8438–8444. doi:10.1002/2014GL061574

Lambert, T., Darchambeau, F., Bouillon, S., Alhou, B., Mbega, J.-D., Teodoru, C. R., et al. (2015). Landscape control on the spatial and temporal variability of chromophoric dissolved organic matter and dissolved organic carbon in large African rivers. *Ecosystems* 18, 1224–1239. doi:10.1007/s10021-015-9894-5

Lawaetz, A. J., and Stedmon, C. A. (2009). Fluorescence intensity calibration using the Raman scatter peak of water. *Appl. Spectrosc.* 63, 936–940. doi:10.1366/000370209788964548

Leenheer, J., Malcolm, R., McKinley, P., and Eccles, L. (1974). Occurrence of dissolved organic carbon in selected ground-water samples in the United States. *J. Res. U. S. Geol. Surv.* 2, 361–369.

Li, P., and Hur, J. (2017). Utilization of UV-vis spectroscopy and related data analyses for dissolved organic matter (DOM) studies: A review. *Crit. Rev. Environ. Sci. Technol.* 47, 131–154. doi:10.1080/10643389.2017.1309186

Li, Y., Song, G., Massicotte, P., Yang, F., Li, R., and Xie, H. (2019). Distribution, seasonality, and fluxes of dissolved organic matter in the Pearl River (Zhujiang) estuary, China. *Biogeosciences* 16, 2751–2770. doi:10.5194/bg-16-2751-2019

Lipczynska-Kochany, E. (2018). Effect of climate change on humic substances and associated impacts on the quality of surface water and groundwater: A review. *Sci. Total Environ.* 640-641, 1548–1565. doi:10.1016/j.scitotenv.2018.05.376

Liu, D., Bai, Y., He, X., Chen, C.-T. A., Huang, T.-H., Pan, D., et al. (2020). Changes in riverine organic carbon input to the ocean from mainland China over the past 60 years. *Environ. Int.* 134, 105258. doi:10.1016/j.envint.2019.105258

López, R., Del Castillo, C. E., Miller, R. L., Salisbury, J., and Wisser, D. (2012). Examining organic carbon transport by the Orinoco River using SeaWiFS imagery. *J. Geophys. Res.* 117, G03022. doi:10.1029/2012jg001986

Mack, J., and Bolton, J. R. (1999). Photochemistry of nitrite and nitrate in aqueous solution: A review. *J. Photochem. Photobiol. A Chem.* 128, 1–13. doi:10.1016/s1010-6030(99)00155-0

Maher, D. T., Santos, I. R., Golsby-Smith, L., Gleeson, J., and Eyre, B. D. (2013). Groundwater-derived dissolved inorganic and organic carbon exports from a mangrove tidal creek: The missing mangrove carbon sink? *Limnol. Oceanogr.* 58, 475–488. doi:10.4319/lo.2013.58.2.0475

Massicotte, P., Asmala, E., Stedmon, C., and Markager, S. (2017). Global distribution of dissolved organic matter along the aquatic continuum: Across rivers, lakes and oceans. *Sci. Total Environ.* 609, 180–191. doi:10.1016/j.scitotenv.2017.07.076

Massicotte, P., and Markager, S. (2016). Using a Gaussian decomposition approach to model absorption spectra of chromophoric dissolved organic matter. *Mar. Chem.* 180, 24–32. doi:10.1016/j.marchem.2016.01.008

McDonough, L. K., Andersen, M. S., Behnke, M. I., Rutlidge, H., Oudone, P., Meredith, K., et al. (2022). A new conceptual framework for the transformation of groundwater dissolved organic matter. *Nat. Commun.* 13, 2153. doi:10.1038/s41467-022-29711-9

McDonough, L. K., O'carroll, D. M., Meredith, K., Andersen, M. S., Brugger, C., Huang, H., et al. (2020b). Changes in groundwater dissolved organic matter character in a coastal sand aquifer due to rainfall recharge. *Water Res.* 169, 115201. doi:10.1016/j.watres.2019.115201

McDonough, L. K., Rutlidge, H., O'carroll, D. M., Andersen, M. S., Meredith, K., Behnke, M. I., et al. (2020c). Characterisation of shallow groundwater dissolved organic matter in aeolian, alluvial and fractured rock aquifers. *Geochimica Cosmochimica Acta* 273, 163–176. doi:10.1016/j.gca.2020.01.022

McDonough, L. K., Santos, I. R., Andersen, M. S., O'carroll, D. M., Rutlidge, H., Meredith, K., et al. (2020a). Changes in global groundwater organic carbon driven by climate change and urbanization. *Nat. Commun.* 11, 1279. doi:10.1038/s41467-020-14946-1

Moona, N., Holmes, A., Wünsch, U. J., Pettersson, T. J. R., and Murphy, K. R. (2021). Full-scale manipulation of the empty bed contact time to optimize dissolved organic matter removal by drinking water biofilters. *ACS Est. Water* 1, 1117–1126. doi:10.1021/acsestwater.0c00105

Moore, W. S., and Joye, S. B. (2021). Saltwater intrusion and submarine groundwater discharge: Acceleration of biogeochemical reactions in changing coastal aquifers. *Front. Earth Sci. (Lausanne).* 9. doi:10.3389/feart.2021.600710

Murphy, K. R., Stedmon, C. A., Wenig, P., and Bro, R. (2014). OpenFluor-an online spectral library of auto-fluorescence by organic compounds in the environment. *Anal. Methods* 6, 658–661. doi:10.1039/c3ay41935e

Nelson, C. E., Donahue, M. J., Dulaiova, H., Goldberg, S. J., La Valle, F. F., Lubarsky, K., et al. (2015). Fluorescent dissolved organic matter as a multivariate biogeochemical tracer of submarine groundwater discharge in coral reef ecosystems. *Mar. Chem.* 177, 232–243. doi:10.1016/j.marchem.2015.06.026

Nelson, N. B., Siegel, D. A., Carlson, C. A., and Swan, C. M. (2010). Tracing global biogeochemical cycles and meridional overturning circulation using chromophoric dissolved organic matter. *Geophys. Res. Lett.* 37. doi:10.1029/2009gl042325

Oh, Y. H., Lee, Y.-W., Park, S. R., and Kim, T.-H. (2017). Importance of dissolved organic carbon flux through submarine groundwater discharge to the coastal ocean: Results from Masan Bay, the southern coast of Korea. *J. Mar. Syst.* 173, 43–48. doi:10.1016/j.jmarsys.2017.03.013

Pain, A. J., Martin, J. B., Young, C. R., Huang, L., and Valle-Levinson, A. (2019). Organic matter quantity and quality across salinity gradients in conduit- vs. diffuse flow-dominated subterranean estuaries. *Limnol. Oceanogr.* 64, 1386–1402. doi:10.1002/lno.11122

Porubsky, W. P., Weston, N. B., Moore, W. S., Ruppel, C., and Joye, S. B. (2014). Dynamics of submarine groundwater discharge and associated fluxes of dissolved nutrients, carbon, and trace gases to the coastal zone (Okatee River estuary, South Carolina). *Geochimica Cosmochimica Acta* 131, 81–97. doi:10.1016/j.gca.2013.12.030

Qi, L., Xie, H., Gagne, J.-P., Chaillou, G., Massicotte, P., and Yang, G.-P. (2018). Photoreactivities of two distinct dissolved organic matter pools in groundwater of a subarctic island. *Mar. Chem.* 202, 97–120. doi:10.1016/j.marchem.2018.03.003

Qu, L., He, C., Wu, Z., Dahlgren, R. A., Ren, M., Li, P., et al. (2022). Hypolimnetic deoxygenation enhanced production and export of recalcitrant dissolved organic matter in a large stratified reservoir. *Water Res.* 219, 118537. doi:10.1016/j.watres.2022.118537

Qu, L., Wu, Y., Li, Y., Stubbins, A., Dahlgren, R. A., Chen, N., et al. (2020). El Niño-driven dry season flushing enhances dissolved organic matter export from a subtropical watershed. *Geophys. Res. Lett.* 47, e2020GL089877. doi:10.1029/2020GL089877

Raymond, P. A., and Spencer, R. G. M. (2015). "Chapter 11 - riverine DOM," in *Biogeochemistry of marine dissolved organic matter*. Editors D. A. Hansell and C. A. Carlson. Second Edition (Boston: Academic Press), 509–533. doi:10.1016/B978-0-12-405940-5.00011-X

Shen, Y., Chapelle, F. H., Strom, E. W., and Benner, R. (2015). Origins and bioavailability of dissolved organic matter in groundwater. *Biogeochemistry* 122, 61–78. doi:10.1007/s10533-014-0029-4

Shen, Y. H. (1999). Sorption of natural dissolved organic matter on soil. *Chemosphere* 38, 1505–1515. doi:10.1016/s0045-6535(98)00371-3

Spencer, R. G. M., Aiken, G. R., Dornblaser, M. M., Butler, K. D., Holmes, R. M., Fiske, G., et al. (2013). Chromophoric dissolved organic matter export from U.S. rivers. *Geophys. Res. Lett.* 40, 1575–1579. doi:10.1002/grl.50357

Stedmon, C. A., Amon, R. M. W., Rinehart, A. J., and Walker, S. A. (2011). The supply and characteristics of colored dissolved organic matter (CDOM) in the arctic ocean: Pan arctic trends and differences. *Mar. Chem.* 124, 108–118. doi:10.1016/j.marchem.2010.12.007

Stedmon, C. A., and Bro, R. (2008). Characterizing dissolved organic matter fluorescence with parallel factor analysis: A tutorial. *Limnol. Oceanogr. Methods* 6, 572–579. doi:10.4319/lom.2008.6.572

Stedmon, C. A., Markager, S., and Kaas, H. (2000). Optical properties and signatures of chromophoric dissolved organic matter (CDOM) in Danish coastal waters. *Estuar. Coast. Shelf Sci.* 51, 267–278. doi:10.1006/ecss.2000.0645

Stedmon, C. A., and Markager, S. (2001). The optics of chromophoric dissolved organic matter (CDOM) in the Greenland Sea: An algorithm for differentiation between marine and terrestrially derived organic matter. *Limnol. Oceanogr.* 46, 2087–2093. doi:10.4319/lo.2001.46.8.2087

Stewart, B. T., Santos, I. R., Tait, D. R., Macklin, P. A., and Maher, D. T. (2015). Submarine groundwater discharge and associated fluxes of alkalinity and dissolved carbon into Moreton Bay (Australia) estimated via radium isotopes. *Mar. Chem.* 174, 1–12. doi:10.1016/j.marchem.2015.03.019

Suryaputra, I. G. N. A., Santos, I. R., Huettel, M., Burnett, W. C., and Dittmar, T. (2015). Non-conservative behavior of fluorescent dissolved organic matter (FDOM) within a subterranean estuary. *Cont. Shelf Res.* 110, 183–190. doi:10.1016/j.csr.2015.10.011

Szymczycha, B., Maciejewska, A., Winogradow, A., and Pempkowiak, J. (2014). Could submarine groundwater discharge be a significant carbon source to the southern Baltic Sea? *Oceanologia* 56, 327–347. doi:10.5697/oc.56-2.327

Tan, E., Wang, G., Moore, W. S., Li, Q., and Dai, M. (2018). Shelf-scale submarine groundwater discharge in the northern South China sea and east China sea and its geochemical impacts. *J. Geophys. Res. Oceans* 123, 2997–3013. doi:10.1029/2017jc013405

Tedetti, M., Cuet, P., Guigue, C., and Goutx, M. (2011). Characterization of dissolved organic matter in a coral reef ecosystem subjected to anthropogenic pressures (La Reunion Island, Indian Ocean) using multi-dimensional fluorescence spectroscopy. *Sci. Total Environ.* 409, 2198–2210. doi:10.1016/j.scitotenv.2011.01.058

Valerio, A. D., Kampel, M., Vantrepotte, V., Ward, N. D., Sawakuchi, H. O., Less, D. F. D., et al. (2018). Using CDOM optical properties for estimating DOC concentrations and pCO_2 in the Lower Amazon River. *Opt. Express* 26, A657–A677. doi:10.1364/oe.26.00a657

Wada, Y. (2016). Modeling groundwater depletion at regional and global scales: Present state and future prospects. *Surv. Geophys.* 37, 419–451. doi:10.1007/s10712-015-9347-x

Walter, J., Chesnaux, R., Cloutier, V., and Gaboury, D. (2017). The influence of water/rock - water/clay interactions and mixing in the salinization processes of groundwater. *J. Hydrology Regional Stud.* 13, 168–188. doi:10.1016/j.ejrh.2017.07.004

Wang, C., Guo, W. D., Guo, Z. R., Wei, J., Zhang, B., and Ma, Z. Y. (2013). Characterization of dissolved organic matter in groundwater from the Coastal Dagu River watershed, China using fluorescence excitation-emission matrix spectroscopy. *Spectrosc. Spectr. Analysis* 33, 2460–2465. doi:10.3964/j.issn.1000-0593(2013)09-2460-06

Wang, C., Guo, W. D., Li, Y., Stubbins, A., Li, Y. Z., Song, G. D., et al. (2017). Hydrological and biogeochemical controls on absorption and fluorescence of dissolved organic matter in the Northern South China Sea. *J. Geophys. Res. Biogeosci.* 122, 3405–3418. doi:10.1002/2017jg004100

Wang, C., Li, Y., Li, Y., Zhou, H., Stubbins, A., Dahlgren, R. A., et al. (2021). Dissolved organic matter dynamics in the epipelagic Northwest Pacific low-latitude Western boundary current system: Insights from optical analyses. *J. Geophys. Res. Oceans* 126, e2021JC017458. doi:10.1029/2021JC017458

Wang, H., Li, Z., Zhuang, W.-E., Hur, J., Yang, L., and Wang, Y. (2020). Spectral and isotopic characteristics of particulate organic matter in a subtropical estuary under the influences of human disturbance. *J. Mar. Syst.* 203, 103264. doi:10.1016/j.jmarsys.2019.103264

Wang, S.-L., Chen, C.-T. A., Huang, T.-H., Tseng, H.-C., Lui, H.-K., Peng, T.-R., et al. (2018). Submarine groundwater discharge helps making nearshore waters heterotrophic. *Sci. Rep.* 8, 11650. doi:10.1038/s41598-018-30056-x

Webb, J. R., Santos, I. R., Maher, D. T., Tait, D. R., Cyronak, T., Sadat-Noori, M., et al. (2019). Groundwater as a source of dissolved organic matter to coastal waters: Insights from radon and CDOM observations in 12 shallow coastal systems. *Limnol. Oceanogr.* 64, 182–196. doi:10.1002/lno.11028

Weishaar, J. L., Aiken, G. R., Bergamaschi, B. A., Fram, M. S., Fujii, R., and Mopper, K. (2003). Evaluation of specific ultraviolet absorbance as an indicator of the chemical composition and reactivity of dissolved organic carbon. *Environ. Sci. Technol.* 37, 4702–4708. doi:10.1021/es030360x

Wünsch, U. J., Murphy, K. R., and Stedmon, C. A. (2015). Fluorescence quantum yields of natural organic matter and organic compounds: Implications for the fluorescence-based interpretation of organic matter composition. *Front. Mar. Sci.* 2. doi:10.3389/fmars.2015.00098

Xiao, Y.-H., Sara-Aho, T., Hartikainen, H., and Vähätalo, A. V. (2013). Contribution of ferric iron to light absorption by chromophoric dissolved organic matter. *Limnol. Oceanogr.* 58, 653–662. doi:10.4319/lo.2013.58.2.0653

Yamashita, Y., Cory, R. M., Nishioka, J., Kuma, K., Tanoue, E., and Jaffe, R. (2010). Fluorescence characteristics of dissolved organic matter in the deep waters of the Okhotsk Sea and the northwestern North Pacific Ocean. *Deep Sea Res. Part II Top. Stud. Oceanogr.* 57, 1478–1485. doi:10.1016/j.dsr2.2010.02.016

Yang, F., Song, G., Massicotte, P., Wei, H., and Xie, H. (2020). Depth-resolved photochemical lability of dissolved organic matter in the Western tropical Pacific Ocean. *J. Geophys. Res. Biogeosci.* 125, e2019JG005425. doi:10.1029/2019JG005425

Yang, L., Chen, C.-T. A., Hong, H., Chang, Y.-C., and Lui, H.-K. (2015). Mixing behavior and bioavailability of dissolved organic matter in two contrasting subterranean estuaries as revealed by fluorescence spectroscopy and parallel factor analysis. *Estuar. Coast. Shelf Sci.* 166, 161–169. doi:10.1016/j.ecss.2014.10.018

Yang, L., Hong, H., Chen, C.-T. A., Guo, W., and Huang, T.-H. (2013). Chromophoric dissolved organic matter in the estuaries of populated and mountainous Taiwan. *Mar. Chem.* 157, 12–23. doi:10.1016/j.marchem.2013.07.002

Zektser, I. S., Everett, L. G., and Dzhamalov, R. G. (2007). *Submarine groundwater*. Boca Raton: CRC Press.

Zhang, Z. G., and Li, L. R. (2005). *Groundwater resources of China (in Chinese)*. Beijing: Sinomap Press.

Zhu, W.-Z., Zhang, H.-H., Zhang, J., and Yang, G.-P. (2018). Seasonal variation in chromophoric dissolved organic matter and relationships among fluorescent components, absorption coefficients and dissolved organic carbon in the Bohai Sea, the Yellow Sea and the East China Sea. *J. Mar. Syst.* 180, 9–23. doi:10.1016/j.jmarsys.2017.12.003

Zsolnay, A., Baigar, E., Jimenez, M., Steinweg, B., and Saccomandi, F. (1999). Differentiating with fluorescence spectroscopy the sources of dissolved organic matter in soils subjected to drying. *Chemosphere* 38, 45–50. doi:10.1016/s0045-6535(98)00166-0